Corrosion Science 137 (2018) 13–32

Contents lists available at ScienceDirect

Corrosion Science

journal homepage: www.elsevier.com/locate/corsci

# Development and characterisation of zinc oxalate conversion coatings on zinc

J.M. Ferreira Jr[a,b,1,*], M. Oliveira[c], G.F. Trindade[b], L.C.L. Santos[a], C.R. Tomachuk[d], M.A. Baker[b]

[a] Federal University of Bahia – Postgraduate Program of Chemical Engineering, R. Prof. Aristides Novis, 2, 2º andar, CEP 40210-630, Federação, Salvador, Bahia, Brazil
[b] Faculty of Engineering and Physical Sciences, University of Surrey, Guildford, Surrey, GU2 7XH, UK
[c] Energy and Nuclear Research Institute, IPEN, CCTM, Av. Prof. Lineu Prestes, 2242, São Paulo, SP, Brazil
[d] Engineering School of Lorena – University of São Paulo, EEL-USP, Environmental and Basic Sciences Department, Lorena, SP, Brazil

ARTICLE INFO

*Keywords:*
A. zinc
A. organic coatings
A. acid solutions
B. EIS
B. XPS
C. passive films

ABSTRACT

The interactions between oxalic acid and zinc substrates have been studied through the deposition of zinc oxalate coating by immersion. The corrosion behaviour of zinc was investigated by surface observation and electrochemical impedance spectroscopy (EIS). Better protective properties were observed for samples treated with $10^{-1}$ M oxalic acid compared to other concentrations and the enrichment of corrosion product by Na was observed. The electrochemical results reveal that the oxalate coating increases corrosion protection in corrosive medium. It is proposed that the zinc oxalate coating formed act as a basis for anchoring zinc corrosion products forming simonkolleite improving corrosion resistance.

## 1. Introduction

One promising class of organic conversion coatings is formed from solutions of (or employ in some manner) carboxylic acids, dicarboxylic acids and salts of these acids. Carboxylic acids are also used as inhibitor solutions and in some cases to promote adhesion when combined with other kinds of materials [1–4]. Even though various investigations have been conducted on the adsorption of carboxylic molecules on metals, a description of the adsorption reaction mechanism and different molecular structures formed is rarely provided. Some studies have shown that the adsorption of oxalic acid (oxalic acid groups), interfacial bonding and the monolayer formed is dependent on the metal employed [5–8]. The important feature of an oxalate is its ability to bind strongly (covalent bond) to many metals, showing different interfacial bonding configurations and improving corrosion protection. Different transition metal-oxalate interfacial ligand coordination arrangements have been synthesized through control of the organic structure or metal functionalisation [9,10]. If improved corrosion protection of the coatings is to be developed, it is therefore important to understand the various parameters which control the oxalate deposition. A simplified description proposed to represent the action of oxalate ions in aqueous media is presented in Eqs. (1)–(3) [11,12]:

$$H_2C_2O_4 \rightarrow H^+ + HC_2O_4^- \rightarrow 2H^+ + C_2O_4^{2-} \quad (1)$$

$$Zn^\circ + 2H^+ \rightarrow Zn^{2+} + H_2 \quad (2)$$

$$Zn^{2+} + C_2O_4^{2-} \rightarrow ZnC_2O_4 \quad (3)$$

However, the deposition of organic molecules is a complex process and depends on the substrate, the treatment solution and the interactions between the organic molecules. The understanding of these interactions would enable the selection of the right molecules for the system which gives the desired properties of the specific carboxyl acid groups or the functionalization of other compounds with these groups [13–15]. Hefny, et al. and some patents have shown zinc passivated after immersion in oxalate media, the dependence between passivation and concentration and zinc oxalate coating mixed with zinc corrosion products [16–18]. The work presented in this paper is part of a wider research programme undertaken to understand the formation mechanism of transition metal oxy-salts. The development of an understanding of the best deposition parameters in the formation of the zinc oxalate coating is essential for building organic coatings with desired architecture. The aim of this work is to investigate different concentrations of oxalic acid solutions for the formation of oxalate with a protective effect for the zinc substrate, characterizing this coating before and after exposure to corrosive medium and to propose a

* Corresponding author.
*E-mail addresses:* jmfj@ufba.br (J.M. Ferreira), m.marcelo@usp.br (M. Oliveira), g.ferraztrindade@surrey.ac.uk (G.F. Trindade), lclsantos@ufba.bra (L.C.L. Santos), celiatomachuk@usp.br (C.R. Tomachuk), m.baker@surrey.ac.uk (M.A. Baker).
[1] Permanent address: Federal University of Bahia – Postgraduate program of Chemical Engineering, R. Prof. Aristides Novis, 2, 2º andar, Federação, CEP 40210-630, Salvador -BA, Brazil.

https://doi.org/10.1016/j.corsci.2018.03.011
Received 29 November 2017; Received in revised form 5 March 2018; Accepted 7 March 2018
Available online 15 March 2018
0010-938X/ 

mechanism to explain the corrosion process in sodium chloride medium. Among the many techniques used to study the adsorption of molecules on metal substrates, X-ray photoelectron spectroscopy (XPS) and time-of-flight secondary ion mass spectrometry (ToF-SIMS) have been successfully used to obtain information of the different surface chemical interactions [19,20]. In this work, the chemical composition and bonding of the surface layers formed on zinc following immersion in an oxalic acid solution of different concentrations was examined by XPS. The surface morphology and elemental composition of the surface layers after and prior to corrosion were also examined using scanning electron microscopy (FEG/SEM), energy dispersive X-ray (EDX) analysis, X-ray diffraction (XRD) and focused ion beam-scanning electron microscopy (FIB/SEM). The corrosion behaviour of the coatings was evaluated by electrochemical impedance spectroscopy (EIS).

## 2. Experimental procedure

### 2.1. Methodology

The salt spray results were used as a way of selecting samples with potential in corrosion protection. Initial results showed better corrosion protection property to samples prepared from oxalic acid conversion solutions with $10^{-1}$ M. The maximum concentration of oxalic acid conversion solution studied was 1 M and therefore the interval between these two concentrations was also studied ($3 \times 10^{-1}$ M, $6 \times 10^{-1}$ M and $9 \times 10^{-1}$ M). However, the best corrosion protection result was always presented by the samples obtained from $10^{-1}$ M oxalic acid confirmed by EIS and salt spray test. That concentration was considered as ideal to the formation of zinc oxalate layer on zinc substrate with best protective corrosion property. The suppression of these results, referent to samples $3 \times 10^{-1}$ M, $6 \times 10^{-1}$ M and $9 \times 10^{-1}$ M, was adopted to make the work linear and simplified.

### 2.2. Substrate

Pure zinc coupons (99.99%) sized 2 cm × 2 cm × 0.2 cm were used as substrates for the treatment with oxalic acid. The zinc surfaces were ultrasonic cleaned in ketone, ethanol and water for 5 min, rinsed in deionized water and dried under a hot air stream for 5 s. After drying, the samples were exposed to air for 2 min to cool down and then immersed in the oxalic acid solutions under mechanical agitation.

### 2.3. Exposure to oxalic acid

The zinc coupons were exposed in oxalic acid solutions of different concentrations. The concentration and pH of the used solutions are shown in Table 1.

Cleaned samples were immersed in these solutions (100 ml per sample) at 25 °C ± 2 °C, under mechanical agitation, for 5 min, then rinsed in deionized water and dried at 90 °C for 15 min.

**Table 1**
Concentration and pH of the investigated oxalic acid solutions.

| $[H_2C_2O_4]$ M | pH |
|---|---|
| $10^{-3}$ | 2.89 |
| $10^{-2}$ | 2.40 |
| $10^{-1}$ | 1.33 |
| $3 \times 10^{-1}$ | 1.13 |
| $6 \times 10^{-1}$ | 1.01 |
| $9 \times 10^{-1}$ | 0.94 |
| 1 | 0.89 |

### 2.4. Surface characterisation

Following immersion in the oxalic acid solution, the samples surface morphology and chemical composition were investigated by SEM-EDX. Those analyses were performed using a Jeol JSM-7100F microscope, employing a Schottky field emission gun, operated at an incident voltage of 15 keV. A Thermo Scientific UltraDry Energy Dispersive Spectrometer (EDX) detector with a NORAN System 7 X-ray Microanalysis System were used to record the elemental maps. The zinc samples after immersing in oxalic acid and dried were scratched with a knife-edge and immediately placed in the electron microscope to obtain chemical maps (EDS). This procedure was adopted to minimize the presence of contaminants by handling and environment exposure.

Glancing incidence angle X-Ray diffraction (XRD) was performed on a PANalytical X'Pert Pro instrument in the diffraction angle range (2θ) 10°–70°, with CuKα radiation source and 1° as incident angle. XPS analysis was carried out on a Thermo Scientific Theta Probe employing a monochromated Al Kα source, operated at 15 keV and 20 mA and using a 400 μm spot size. For all spectra, a 0.2 eV step size was employed. XPS survey spectra were acquired at a pass energy of 100 eV and core level (C1s, O1s, Zn2p, Na1s, Cl2p) narrow scans recorded using a pass energy of 50 eV. A low-energy electron flood gun was used for charge compensation. Quantitative chemical compositions were calculated from the high-resolution core level spectra, following the removal of a nonlinear Smart background and use of instrument modified sensitivity factors. To investigate changes in chemical composition as a function of depth through the oxalate coating, XPS depth profiles were undertaken. Sputtering was performed using 3.0 keV $Ar^+$ ions and a beam current of 1 μA with a raster size of 3 mm × 3 mm to minimize effects of charging at the insulating films, a low-energy electron gun was used for charge neutralization. Concentration calculation was done using single-element standard sensitivity factors and assuming a homogeneous mixture of the elements in the analysis region.

ToF-SIMS analysis was performed on a TOF.SIMS 5 system from ION-TOF GmbH (Muenster, Germany) using a 25 keV $Bi_3^+$ ion beam operated in the high current bunched mode delivering 0.3 pA, pulsed at 10 kHz and rastered over regions of 100 × 100 $\mu m^2$. Three different regions were analysed for each sample and positive ions spectrum were acquired for 60 s each. All the data were recorded within the static SIMS limit of $10^{13}$ ions/$cm^2$/analysis. The spectra were calibrated using a unique calibration peak list containing characteristic zinc oxide peaks [21,22]. The isotopic distributions of fragments provided enough calibration points to achieve precise peak assignments.

FIB analysis was carried out using an FEI Nova 600 NanoLab Dual Beam FIB system, which is comprised of rastered gallium ion beam and a high-resolution field emission scanning electron microscope. The focused $Ga^+$ ion beam was operated at an energy of 5–30 keV and probe current of 1 pA–20 nA. The $Ga^+$ ion beam resolution is 7 nm when employing at 1 pA beam current and 30 keV accelerating voltage. The beam spot size and resolution vary with the ion beam current. Electron optics consists of a high-resolution field emission SEM column. The acceleration voltage can be adjusted continuously from 0.2 to 30 kV and the beam current increased up to 20 nA in 21 steps. The stage was tilted at an angle of to 38° to the incident electron beam. During the writing process the stage is stationary, and only the beam scans the sample surface. The ion beam is focused on the sample surface with a normal incident angle.

#### 2.4.1. XPS peak fitting

C 1 s peak fitting was carried out with the C 1s peak assignments for different components as following: peak I (285.0 eV ± 0.1 eV), adventitious carbon (C—C/C—H); peak II (285.7 ± 0.1 eV), β carbon (—C—COOx); peak III (286.8 eV ± 0.1 eV), carbon in carbonyl (—C—O); peak IV (289.0 eV ± 0.1 eV), carbon in carboxyl (—O—C═O—); and peak V (290.1 eV ± 0.1 eV), carbonate groups and/or adsorbed CO and $CO_2$ (C═O) [23–25]. Curve fitting of the O 1 s spectra

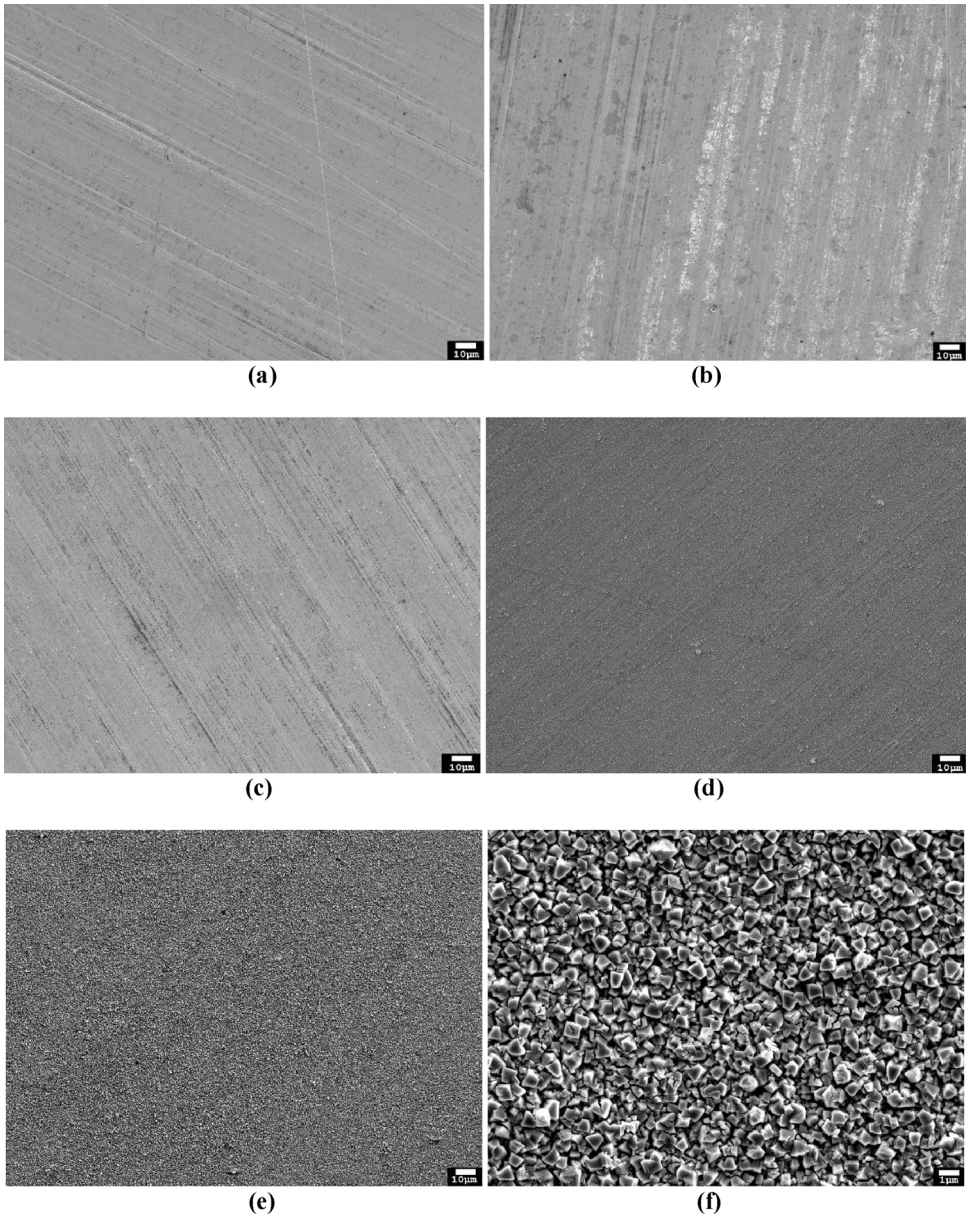


**Fig. 1.** SEM images of zinc surfaces: (a) Zinc surface untreated; and after immersion for 5 min in oxalic acid solutions with (b) $10^{-3}$ M; (c) $10^{-2}$ M; (d) 1 M; (e) $10^{-1}$ M and (f) $10^{-1}$ M (with different magnification).

yielded the following peaks: peak I (530.5 ± 0.1 eV), oxide; peak II (532.1 ± 0.1 eV) hydroxide; peak III (533.1 ± 0.1 eV) carboxyl groups, carbon dioxide and/or adsorbed water [24,25]. For Zn 2p3/2 peaks, the curve fits gave the following three peaks: peak I (1021.2 ± 1.6 eV) metallic zinc, peak II (1022.1 ± 1.6 eV) zinc oxide and peak III (1023.9 ± 1.6 eV) zinc hydroxide and/or carbonate. Other authors report the difficulty in differentiating the various chemical states for the zinc peak (Zn 2p3/2). More reliable peak assignments can be obtained when the Zn 2p peaks are considered together with the Zn Auger $L_3M_{45}M_{45}$ peak to yield the Auger parameter. Zn $L_3M_{45}M_{45}$ Auger peak fitting was made using four peaks with the following kinetics energies: peak I (987.7 ± 2.3 eV), peak II (989.9 ± 2.3 eV), peak III (992.6 ± 2.3 eV) and peak IV (996.1–998.5 eV). Peaks I and II correspond to zinc oxide and peaks III and IV to metallic zinc [26,27].

Depth profiles were obtained at different levels; with each level corresponding to 150 s etch. That is, 150 s of argon ion sputtering.

### 2.5. Electrochemical measurements

The experimental set up consisted of a three-electrode in a horizontal cell arrangement with an Ag/AgCl, KCl saturated electrode and a platinum wire used as the reference and counter electrodes, respectively. The working area of the electrode (zinc samples with the various surface treatments tested) exposed to the electrolyte corresponded to 1 $cm^2$. The electrolyte used in the corrosion tests was sodium chloride solution (200 ml) with concentration $10^{-1}$ M, quiescent, aerated and at (22 ± 3) °C. The electrochemical behaviour of the surfaces tested was monitored by electrochemical impedance spectroscopy (EIS) measurements carried out in the frequency range from 100 kHz to 10 MHz, with a signal amplitude perturbation of 10 mV, and data acquisition rate of 10 points per decade. EIS data was acquired in the potentiostatic mode at the open circuit potential (OCP), using a BioLogic SP200 potentiostat controlled by EC-Lab V23.10 software. The EIS tests were performed after the stabilization of the open potential circuit (3 h). The results were adjusted according to equivalent electric circuits using the software Zview version 3.1

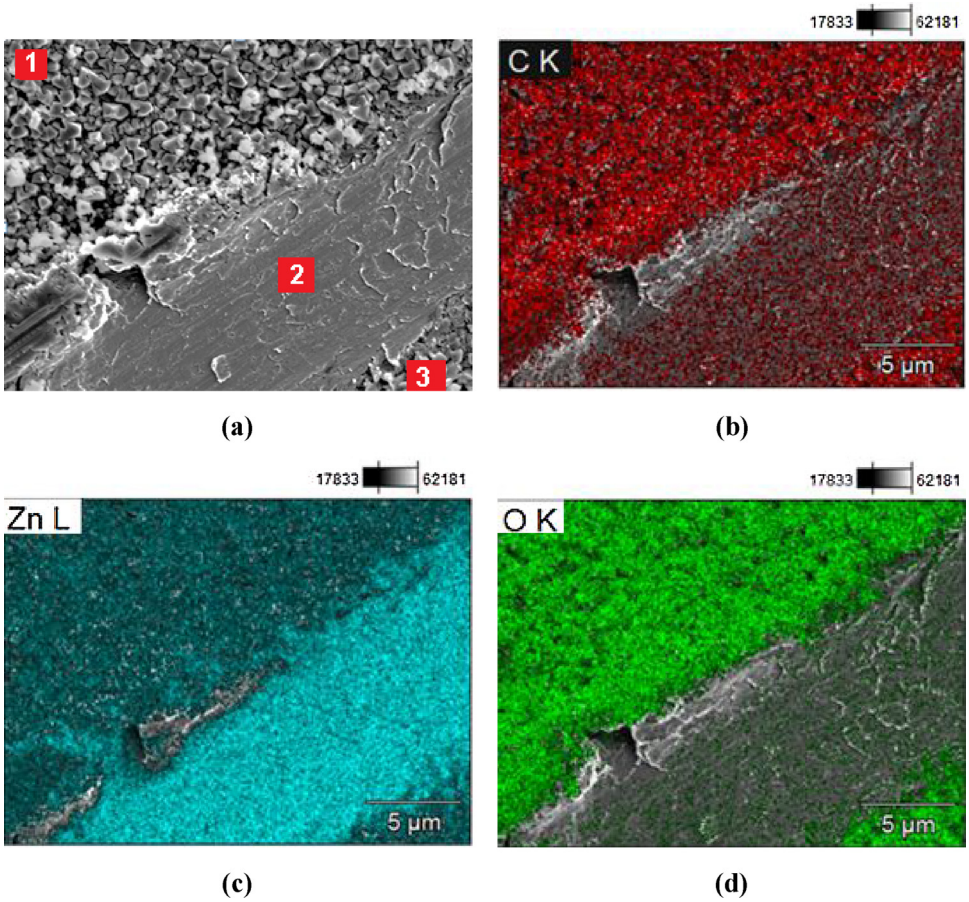


**Fig. 2.** SEM/EDX elemental maps of the zinc surface after immersion in $10^{-1}$ M oxalic acid solution for 5 min. (a) regions 1, 3 preserved and 2 scratched with a knife-edge; (b) carbon; (c) zinc and (d) oxygen.

### *2.6. Salt spray test*

ASTM B117 salt spray tests (ASTM B117, 2016) were performed in an accelerated corrosion chamber, which provides a corrosive controlled environment in the form of a 5% m/v NaCl solution. Prediction of performance in natural environments was rarely correlated with salt spray results when used as isolated data [28]. However, this is one of the most accepted assays by industries in the evaluation of surface corrosion resistance. The reproducibility of the results is highly dependent on the type of samples tested and the selected evaluation criteria, as well as the control of the operational variables. In a test program, sufficient replicates should be included to establish the variability of the results. The salt spray test was used as a preliminary evaluation method to select treatment with better corrosion protection compared to zinc substrate. The tests were performed in triplicate with border samples protected by plastic tape, to prevent edge corrosion, according to standard ABNT NBR 11003, samples dimensions with waterproof adhesive tape (9.5 cm × 4.5 cm × 0.01 cm) and without tape (10 cm × 5.0 cm × 0.01 cm).

## 3. Results and discussion

### *3.1. Before exposure to 10–1 M NaCl solution (corrosion test)*

#### *3.1.1. Morphology*

SEM micrographs of the zinc surfaces, untreated and after treatment in oxalic acid solutions with concentrations of $10^{-3}$ M, $10^{-2}$ M, 1 M and$10^{-1}$ M are shown, respectively in Fig. 1 (a–f).

Morphology and microstructure of the zinc oxalate is composed of mainly prismatic particles with approximately 1 μm size range, which is a similar morphology to the one described by Sinha et al. [29]. Coolant cold rolling of the zinc sheets results in the formation of grooves in the surface, as shown in Fig. 1(a). These grooves were still visible on the surfaces treated in $10^{-3}$ M and $10^{-2}$ M oxalic acid solutions, meaning that these concentrations were not effective in coating deposition. For the coating deposited from the 1 M oxalic acid solution, theses grooves are barely visible and for the $10^{-1}$ M oxalic acid solution, no grooves can be seen. This observation suggests that the deposited coating thickness increases with oxalic acid concentration up to $10^{-1}$ M, where the defect coverage is maximum. In the case of the 1 M concentration, there is the formation of a coating, but the lines of the zinc substrate are still visible. Moreover, it has been observed presence of small pits on the surface indicating surface attack in low concentration of oxalic acid and in the maximum oxalic acid concentration used ($10^{-3}$ M, $10^{-2}$ M and 1 M) without effective coating deposition. The results suggest that there is a competition between zinc dissolution in the acid medium and the deposition of zinc oxalate ion that is dependent on the oxalate and hydrogen ions concentration at the zinc surface. The surface of a sample exposed to the $10^{-1}$ M oxalic acid solution was scratched with a knife-edge and immediately analysed revealing the underlying Zn substrate. The EDX elemental maps of carbon, zinc and oxygen were recorded on the scratched area and surrounding regions (Fig. 2).

Fig. 2a shows that the grains are uniformly distributed and give rise to a porous coating. In addition, the scratch removed the coating, exposing the underlying substrate. High carbon and oxygen concentrations were observed in regions 1 and 3, (Fig. 2b and d) where the coating is intact, suggesting the formation of an oxalate coating. The underlying zinc substrate is clearly visible in region 2 (Fig. 2c). Although scratched has been made and the sample immediately inserted into the microscope it is possible to observe contaminant carbon in the

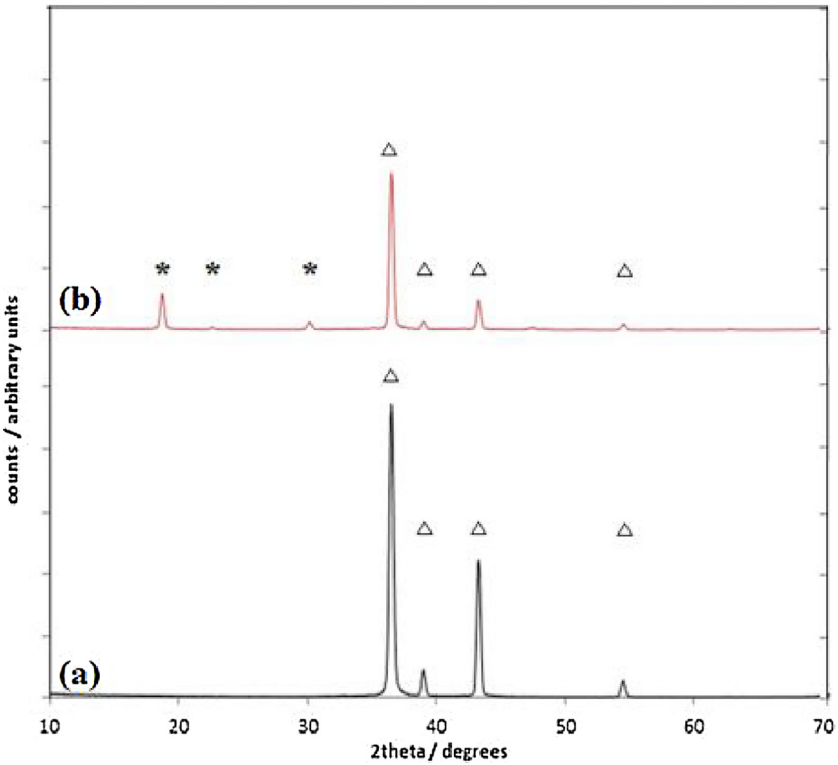


**Fig. 3.** XRD diffractograms obtained from (**a**) the untreated zinc surface **(b)** from the zinc surface after immersion in $10^{-1}$ M oxalic acid solution for 5 min.

defect region. The discrepancy between the carbon signals in defect and intact areas illustrates the difference between the oxalate coating and the contaminated region.

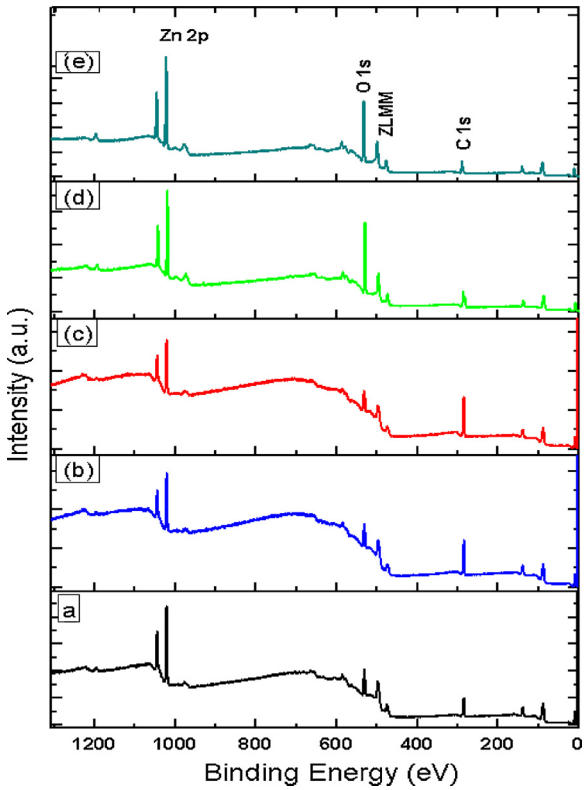


**Fig. 4.** XPS survey spectra from: (a) untreated zinc; zinc samples treated in oxalic acid solutions at concentrations of: (b) $10^{-3}$ M; (c) $10^{-2}$ M; (d) $10^{-1}$ M and (e) 1 M, respectively.

*3.1.2. Chemical and structural characterization*

*3.1.2.1. XRD.* The XRD diffractograms for the zinc samples untreated and treated by immersion in oxalic acid solution $10^{-1}$ M for 5 min are shown in Fig. 3.

Peaks from the underlying Zn (**Δ**) are present in both samples diffractograms. Peaks of hydrated zinc oxalate ($ZnC_2O_4.2H_2O$) at 18.5°, 22.6° and 30.2° (*) are observed on the treated surface, confirming the deposition of a crystalline zinc oxalate layer on the zinc surface by immersion in the $10^{-1}$ M oxalic acid solution. The peak widths indicate crystallization of the coating formed, however, the peaks of ZnO and Zn $(OH)_2$ which could be expected from zinc substrate were not observed.

*3.1.2.2. XPS.* Fig. 4 shows the XPS survey spectra for untreated zinc and the zinc samples treated in oxalic acid solutions with increasing concentration.

In the survey spectra, three main observations can be made for the samples treated at the two highest oxalic acid concentrations (and untreated zinc) compared to that for the two lowest: (i) the Zn/O peak intensity ratio is much lower; (ii) the C 1s peak has a much lower intensity; (iii) the background signal associated with the Zn 2p and Zn LMM peaks is decreased. The high-resolution scan data for Zn 2p, C 1s, O 1s and Zn LMM peaks are presented in Fig. 5.

The C 1s peaks for the untreated and treated samples in solutions $10^{-3}$ M and $10^{-2}$ M show a very similar peak shape with the main component being clearly the C—C/C—H peak at 285.0 eV. Hence, at these low oxalic acid concentrations, zinc oxalate formation is not favoured. Exposure to higher oxalic acid concentrations ($10^{-1}$ M and 1 M) resulted in carbon peaks of very different shapes, with the main peak now appearing at a binding energy of 289.4 eV. This peak can be divided into two components, (289 eV) carbon in carboxyl (—O—C═O—) ascribed to zinc oxalate and/or in carbonate groups adsorbed CO and $CO_2$ (C═O) and (290.1 eV) carbon. A peak at this binding energy is often reported as showing evidence of bonding between carboxylic groups and various metal surfaces such as iron, magnesium, aluminium and zinc [30–34]. These results show that immersion in solutions of oxalic acid of lower concentration ($10^{-3}$ M and $10^{-2}$ M) promote the

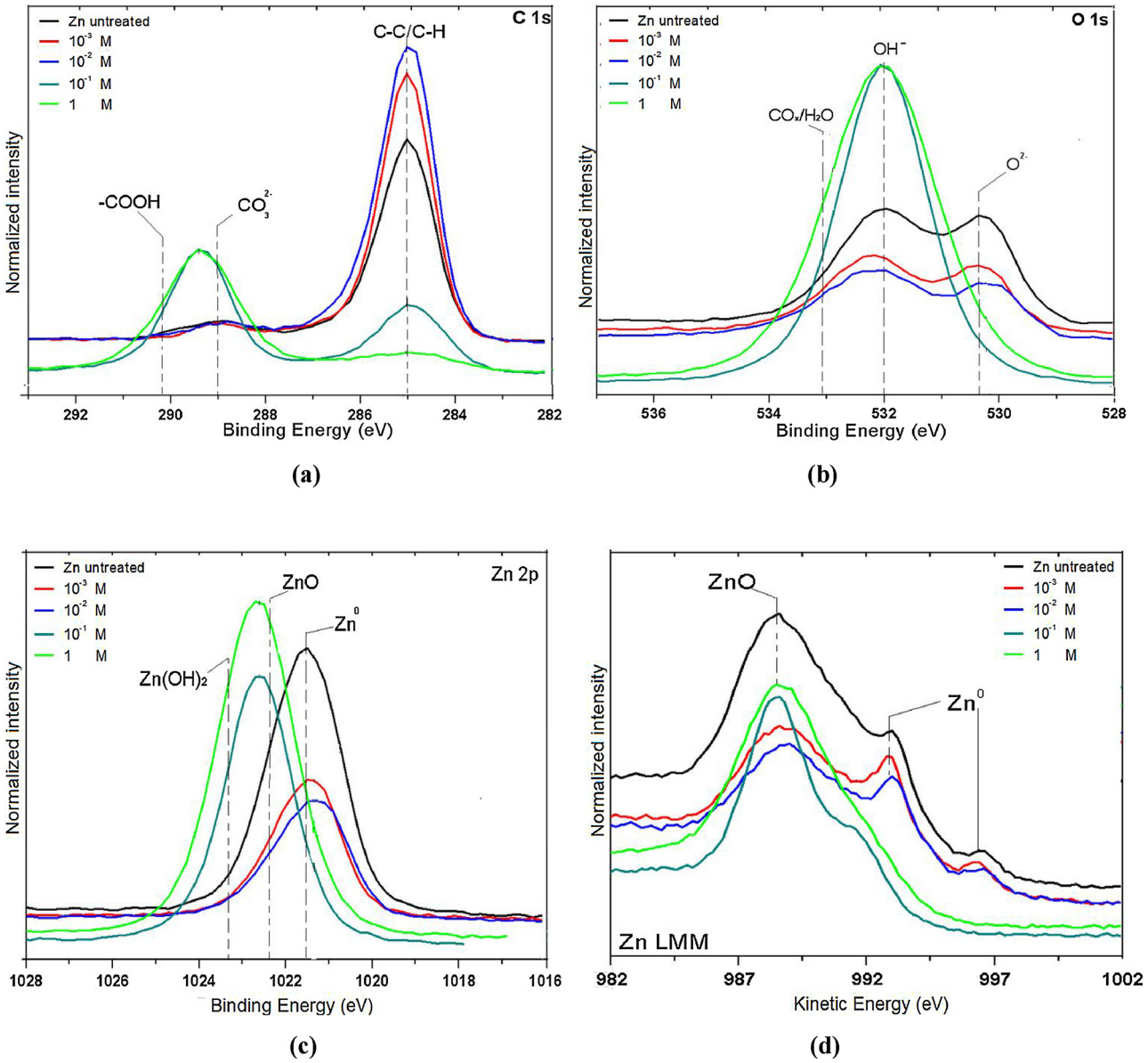


**Fig. 5.** Overlay of XPS high resolution spectra and peak positions for: (a) carbon (C 1s); (b) oxygen (O 1s); (c) zinc (Zn 2p3/2) and (d) zinc auger (Zn $L_3M_{45}N_{45}$).

attack of the surface with the formation of carbonate and the higher concentrations (1 M and $10^{-1}$ M) allow the deposition of zinc oxalate (see Fig. 1).

Analogous to the C 1s peak, the O 1s peak shows a very similar behaviour between the untreated samples and the samples treated in oxalic acid solution with $10^{-3}$ M and $10^{-2}$ M, there being two strong peaks at binding energies of 530.2 eV and around 532.0 eV. For samples treated in solutions of $10^{-1}$ M or 1 M oxalic acid, only the peak at 532.0 eV is observed and it corresponds to ZnO [32–34]. The peak at 532.0 eV can be either ascribed to $Zn(OH)_2$ for the untreated zinc and samples treated in oxalic acid solutions with $10^{-3}$ M and $10^{-2}$ M, or to zinc oxalate for zinc samples exposed to solutions with $10^{-1}$ M or 1 M of oxalic acid.

The XPS Zn $2p_{3/2}$ spectra for untreated zinc samples and samples treated in $10^{-3}$ M or $10^{-2}$ M solutions show a peak at 1021.5 eV, corresponding to Zn/ZnO. The peak has a shoulder at higher binding energies, associated with the presence of $Zn(OH)_2$ and/or $ZnCO_3$, in agreement with the O 1s spectrum. However, the surfaces treated in more concentrated solutions ($10^{-1}$ M and 1 M), present only a single component, which can be ascribed to zinc oxalate.

The Zn Auger LMM peak revealed the presence of three peaks for samples untreated and treated in $10^{-3}$ M and $10^{-2}$ M solutions. These peaks are related to metallic zinc and were not detected for the samples treated in the $10^{-1}$ M and 1 M solutions. This is due to the thicker coatings formed in the more concentrated solutions and these results agree with the morphology results. The binding energies and quantified concentrations associated with the C, O and Zn peaks are presented in Table 2.

*3.1.2.3. ToF-SIMS.* Two main positive ion fragments were considered in order to track the possible binding modes of COOH or COO− groups to metal oxides. The fragment $C_2O_3Zn^+$ for monodentate or bidentate chelating and $C_2O_4Zn^{2+}$ for bidentate bridging. The molecular ion $[M{-}OH]^+$ for the oxalic acid and a zinc carbonate fragment, $CO_2Zn^+$, were also selected. The structures of the fragments and their respective deviations from exact masses after peak assignment are present in Table 3. Fig. 6 shows the high-resolution view of the selected peaks. All spectra were binned down to 100,000 channels and submitted to a moving average smoothing function.

One could consider using daughter fragments of the ones shown in

**Table 2**
XPS peak binding energies and elemental concentrations observed for the untreated zinc and zinc immersed in oxalic acid solutions of varying concentration.

| Treatment | XPS peak | BE (eV) | Elemental concentration (at. %) |
|---|---|---|---|
| **Zinc untreated** | **C 1 s** | 285.0 | 46.50 |
| | **O 1 s** | 532.0 | 32.50 |
| | **Zn 2p3/2** | 1021.5 | 21.00 |
| **Zinc in $10^{-3}$ M Oxalic acid** | **C 1 s** | 285.0 | 63.60 |
| | **O 1 s** | 532.2 | 24.10 |
| | **Zn 2p3/2** | 1021.3 | 12.30 |
| **Zinc in $10^{-2}$ M Oxalic acid** | **C 1 s** | 285.0 | 68.60 |
| | **O 1 s** | 532.2 | 20.80 |
| | **Zn 2p3/2** | 1021.4 | 10.60 |
| **Zinc in $10^{-1}$ M Oxalic acid** | **C 1 s** | 289.4 | 47.40 |
| | **O 1 s** | 532.0 | 46.50 |
| | **Zn 2p3/2** | 1022.8 | 6.10 |
| **Zinc in 1 M Oxalic acid** | **C 1 s** | 289.4 | 46.60 |
| | **O 1 s** | 532.0 | 48.40 |
| | **Zn 2p3/2** | 1022.8 | 5.00 |

Table 3 (mainly fragments containing one carbon atom) as their peak intensities are much higher and therefore easier to identify in the mass spectra. However, the choice of the former instead of the fragments containing two carbon atoms would create a series of ambiguities, since further fragmentation of the peaks considered leads to the structures in-common. Fig. 7 shows the intensities of the selected peaks (normalised by total counts of the peak list) in function of treatment concentration.

It can be observed that for lower concentrations of oxalic acid treatment, there is relative predominance of zinc carbonate (green line). As the concentration of oxalic acid increases to $10^{-1}$ M, the mono/bidentate become the predominant binding modes (red line). For the highest concentrations, the bidentate bridging becomes predominant together with mono/bidentate (black and red lines). The decrease of the oxalic acid $[M\text{-}OH]^+$ ion intensity (blue line) indicates that higher concentrations favour the intended carboxylate-oxide bonds.

Fig. 7 shows only relative areas and it is important to mention that the signals of the considered peaks are extremely low (approximately 1% of the Zn + peak) and could only be detected because ToF-SIMS is an extremely sensitive technique. These results combined with the XRD and XPS results, shown sequentially, allowed to characterize the coating formed as zinc oxalate and will be designated as such in the next sessions.

### 3.2. Corrosion test

#### 3.2.1. Salt spray test

Salt spray tests were previously used to select treatments with higher corrosion resistance. Sequentially the selection of zinc oxalate $10^{-1}$ M and 1 M as more protective treatments and cleaned zinc samples, zinc oxalate $10^{-1}$ and zinc oxalate 1 M, were analysed by salt spray test as condition of comparison. The results of the salt spray tests for these samples exposed up to 172 h are shown in Fig. 8.

The effect of the treatment in $10^{-1}$ M and 1 M oxalic acid solution resulting in surfaces with less amount of corrosion products is indicated up to 24 h, but for 72 h of the corrosion protection effect of the coating formed is only indicated for treatment $10^{-1}$ M oxalic acid. For this test

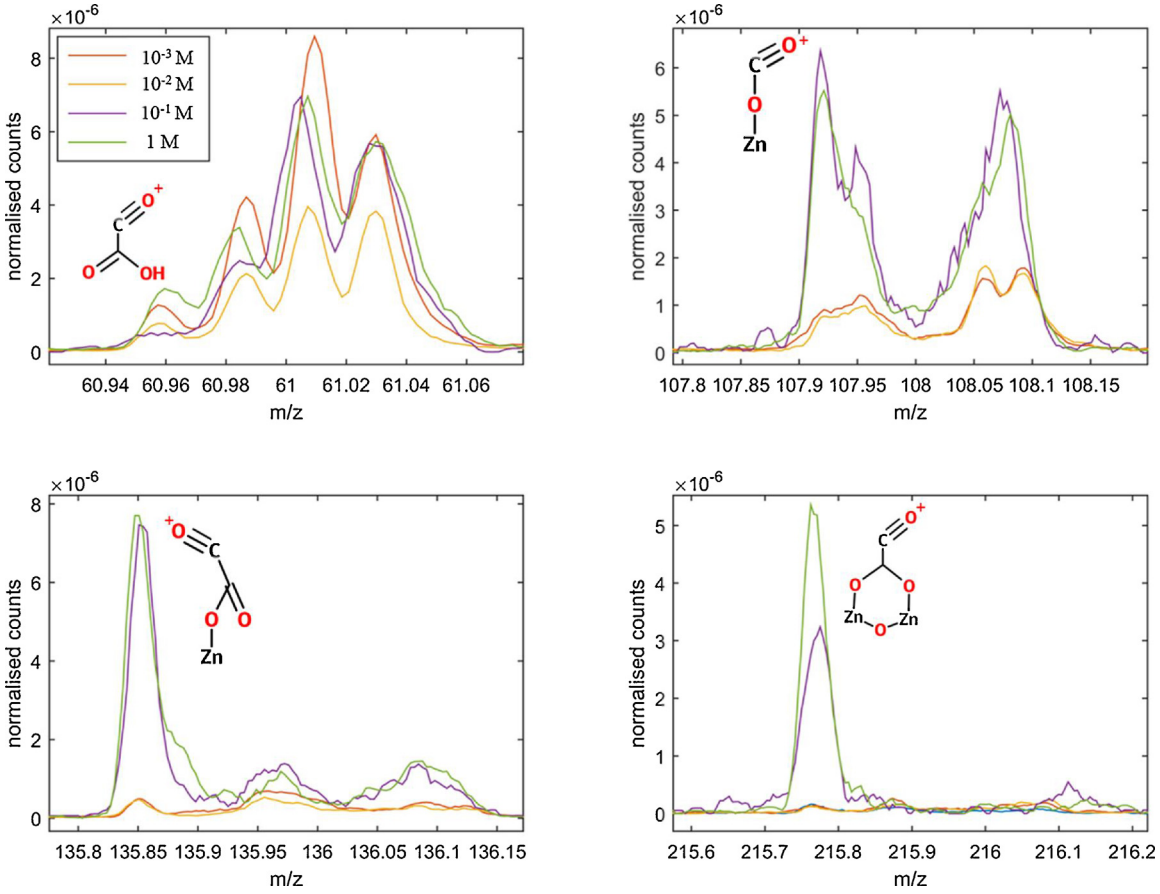


**Fig. 6.** ToF-SIMS selected peaks for the different treatment concentrations.

**Table 3**
ToF-SIMS fragments, structures and their respective deviations from exact masses after peak assignment.

| Assignment | Exact mass (u) | Deviation (ppm) | Structure |
|---|---|---|---|
| **[M-OH]$^-$ Carboxylic acid** | 60.99 | 1.4 |  |
| **$CO_2Zn^+$ Zinc carbonate** | 107.91 | 98 |  |
| **$C_2O_3Zn^+$ Monodentate bidentate chelanting** | 135.91 | −61.2 |  |
| **$C_2O_3Zn^{2+}$ Bidentate bridging** | 215.84 | −68.9 |  |

period, the quantity of products is higher for the sample treated in solution with 1 M oxalic acid than the untreated surface (Zn). This behaviour is confirmed for 120 h of exposure to the salt spray test and, only after 172 h of the test, bulky corrosion products were observed on the treated surface with $10^{-1}$ M oxalic acid. This result evidences the higher protection efficiency to oxalate coating formed from oxalic acid solution $10^{-1}$ M in relation to samples prepared from 1 M.

### 3.2.2. Electrochemical characterization (EIS)

The evolution of the electrochemical behavior at the surface of the untreated zinc and zinc with the oxalate coating formed in the oxalic acid solution was monitored by electrochemical impedance spectroscopy (EIS) as a function of time in open circuit potential (ocp). The aim was to compare the effect of the oxalate coating on the corrosion resistance of the zinc surface. The EIS results Nyquist and Bode diagrams for both types of zinc surface, untreated and treated ($10^{-1}$ M), are presented in Fig. 9 for periods of exposure corresponding to 4 h, 1 day, 3 days, 5 days and 7 days in $10^{-1}$ M NaCl solution.

The results corresponding to 4 h of exposure show a time constant corresponding to frequencies of around 10 Hz likely due to charge transfer processes and charging of the double layer at the zinc surface and underneath the pores in the oxalate layer. Lower impedances were related to the surface treatead in $10^{-1}$ M oxalic acid. A small tail is indicated at lower frequencies likely due to the formation of corrosion products on the surface. This hypothesis is supported by the results obtained at 1 day and 3 days of test for the untreated zinc surface. The deposition of corrosion products on the surface is also indicated by a shoulder at higher frequencies for the zinc untreated surface. For 1 day of exposure, the indication of another time constant at low frequencies associated to corrosion processes at the metallic substrate is seen on the Nyquist diagram. The phase angle around 22° could be due to a diffusion controled corrosion process through the porous corrosion products deposited on the zinc surface.

The electrochemical behavior of the Zn treated surface at low frequencies for periods of immersion test until 3 days show distinct characteristics from the untreated zinc. For the first type of samples, only a time constant is evident from the diagrams indicative of charge transfer processes coupled to charging of the double layer. Seemingly the oxalate layer obtained in the $10^{-1}$ M oxalic acid solution does not have a barrier effect to the access of electrolyte. On the other hand, the air formed zinc oxide seems to offer protection to the corrosive attack from the solution. It must be mentioned that the zinc oxide film is removed from the zinc surface during treatment in the oxalic acid solution before the formation of zinc oxalate coating.

In fact, during the treatment there is a competition between the corrosive attack of the zinc oxide surface and the precipitation of zinc oxalate. However, it is interesting to note that for 5 days of exposure the impedances associated to the treated surface were much superior to that of the untreated one. This result shows that between 3 days and 7 days of exposure there was a large increase in the impedance of the treated surface whereas that of the untreated one decreased. This could be explained by the activation of localized sites at the untreated zinc. In fact, intense localized corrosion was seen at the untreated zinc surface, whereas an uniform and generalized attack was found at the surface of the treated ones, as shown in Fig. 8.

The Bode diagrams corresponding to 5 days and 7 days of immersion test are very similar. Both show a shoulder at frequencies around 10 Hz and a peak at 1 Hz indicating a stable surface after the increasing removal of the oxalate coating. In addition, it is necessary consider that attack by corrosive medium changed part of the zinc oxalate coating to sodium oxalate and sodium carbonate, more protective.

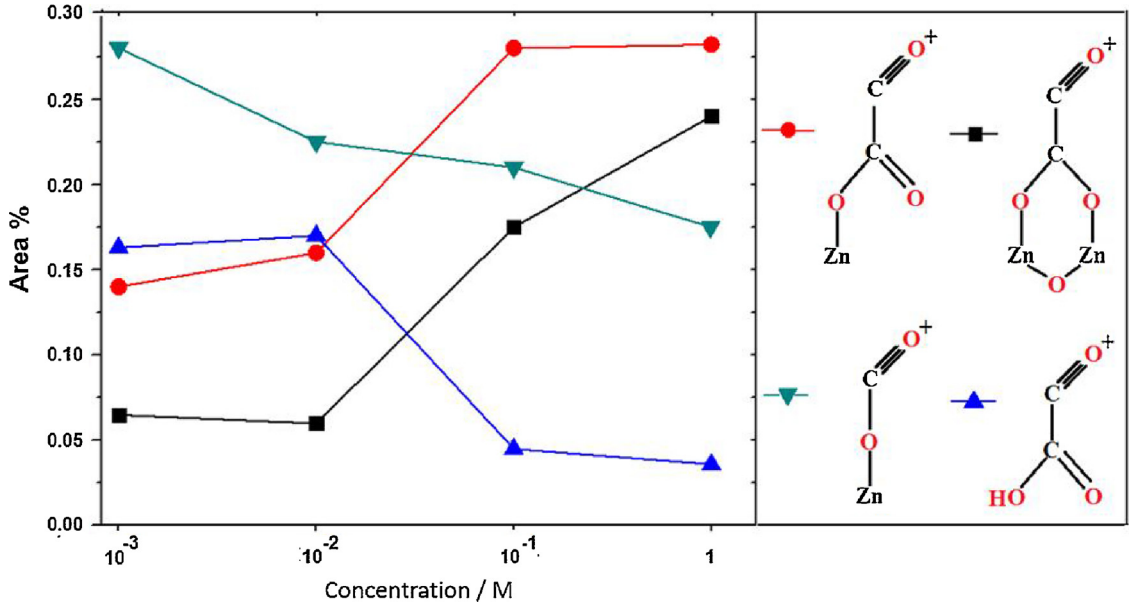


**Fig. 7.** ToF-SIMS selected peak intensities in function of treatment concentration (For interpretation of the references to colour in the text, the reader is referred to the web version of this article).

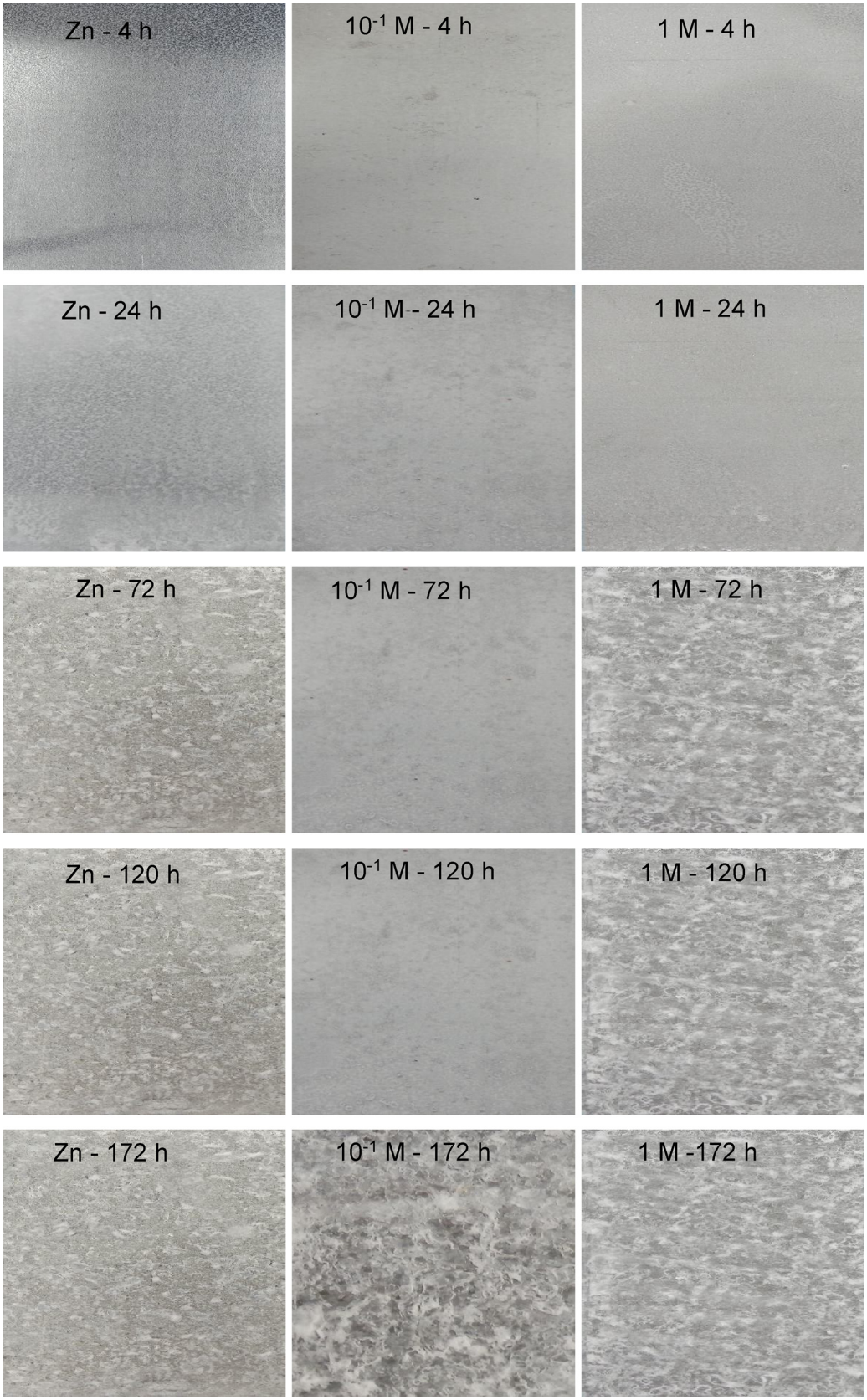


**Fig. 8.** Surface of untreated zinc (Zn) and zinc oxalate $10^{-1}$ M and 1 M after several exposure times (up to 172 h) in the salt spray test (ASTM B117).

To quantify and better understand the changes in the impedance plots for zinc samples untreated and with oxalate coating, the results were adjusted by circuit electric equivalent [35,36]. The results presented in Fig. 9 were fitted using a typical circuit electric equivalent (CEE) to zinc untreated (a) and oxalate coating ($10^{-1}$ M). The circuit includes two-time constants up to 7 days of immersion into chloride

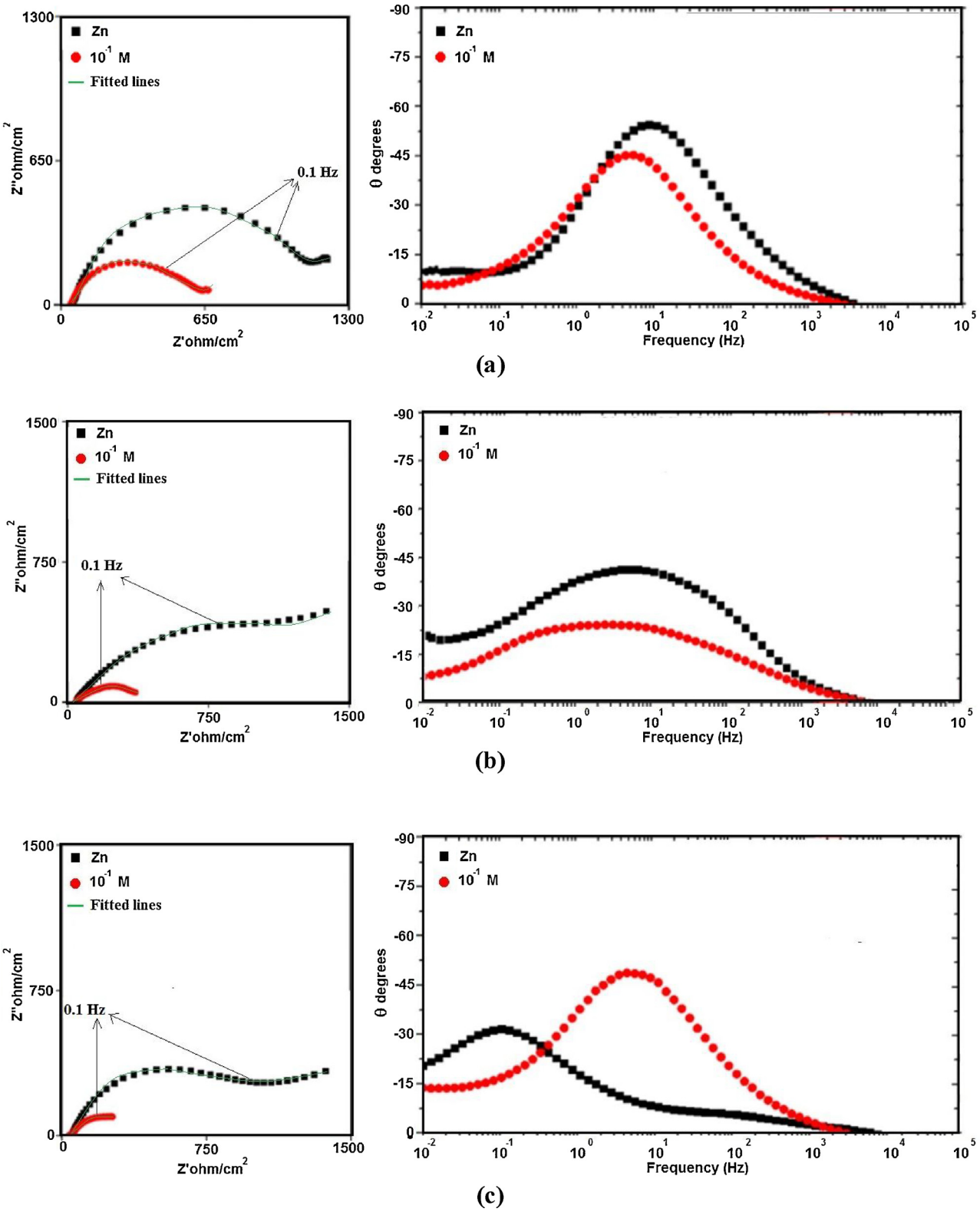


**Fig. 9.** EIS results for untreated zinc (Zn) and treated (5 min of immersion in $10^{-1}$ M oxalic acid) and then exposed to $10^{-1}$ M NaCl solution for (a) 4 h; (b) 1 day; (c) 3 days; (d) 5 days and (e) 7 days.

solution and Warburg element to zinc untreated, as shown in Fig. 10.

In the equivalent circuit of Fig. 10, the resistive terms $R_{sol}$, $R_{ct}$ ($R_1$) and $R_{dl}$ ($R_2$) account for the electrolyte, intermediate layer and interfacial resistance, respectively. The element $CPE_1$ is related to the properties of the protective layer, and the element $CPE_2$ is related to the double layer capacity. The α values represent values of a typical resistance (α = 0), a Warburg element $W_1$ (α = 0.5), an ideal capacitor (α = 1) and an idutor (α = −1) [37–39]. The accquired values to fitting procedures showed errors inferior to 10%, presented on Table 4.

Nyquist plot in Fig. 9 showed three apparent capacitive arcs after all times of exposure for zinc untreated. After 4 h exposure, the Nyquist plot exhibited Warburg impedance in the low frequency region, which

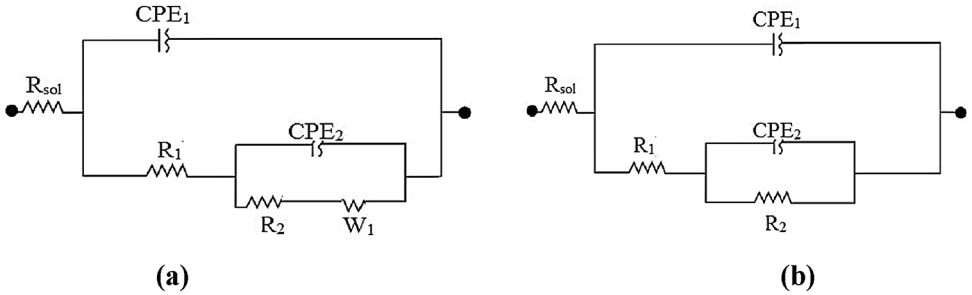


**Fig. 10.** Circuit electric equivalent obtained after exposure to $10^{-1}$ M NaCl solution up to 168 h to (a) zinc untreated and (b) zinc oxalate $10^{-1}$ M.

revealed that a diffusion-controlled corrosion process occurred on the zinc surface. The frequency response of this electric circuit depend on the mutual weight between charge transfer resistance ($R_1$) and resistance to oxygen diffusion (Zw). In the case of the studied Rct < Zw for all analyzed times [39].

This diffusion process could be attributed to the formation of insoluble corrosion products, which blocked the mass transfer process of the corrosion reactions. For the Fig. 9a, the angular value of the line which corresponded to the Warburg impedance in the low frequency region of the Nyquist plot was lower than $\pi/4$ after 4 h of exposition.

The value of resistance solution ($R_{sol}$) decreases up to 5 days, during longer corrosion assigning the increase in zinc ion concentration to the zinc solubilisation process. However, after 7 days resistance becomes highest showing a decrease of ionic species in a solution. The passive zinc layer on the electrode surface is thin and the dissolution of corrosion products and transport of species are depressed after 5 days of exposure to chloride solution.

The low values presented by $CPE_1$ after immersion times of 4 h, 1 day and 3 days are typical of porous films. After 5 days, the highest value is noticed, indicating the formation of poorly soluble corrosion products and possibly forming a layer consisting of these products. This argument is supported by values of the α1 constant. The value associated with 3 days is typical of diffusional processes, showing that the zinc corrosion products have dissolved. After the dissolution of zinc corrosion products, new products with lower solubility were formed. The zinc corrosion mechanism undergoes a significant change after this period of immersion in chloride solution.

Generally, corrosion resistance decreases to a minimum value after a few hours of immersion due to the disruption of the air layer formed on the zinc oxide film. Subsequently, the corrosion resistance increases slowly at first day of immersion with corrosion products formation. The oxide passive film is broken and, from the third day, the electrolyte solution penetrates it and starts the formation of new corrosion products. Finally, it remains almost stable after 5 days due to the accumulation of corrosion products that can still difficult corrosion even more. The corrosion products are mainly composed of ZnO, $Zn(OH)_2$ and $Zn_5(OH)_8Cl_2$ [37–39]. The obtained values from electrochemical fitting procedures had errors inferior to 10%, the fitting values to zinc oxalate coating are shown in Table 5.

The equivalent circuit for the coatings showed its basic structure and the adjusted values showed changes in the regularity of the structure with increase of immersion time. The resistance of the solution ($R_{Sol}$) decreased with the increase of oxidation time, which can be related to the state change of the surface coating (such as porosity or the actual surface area). Corrosion products increased with the oxidation time and the surface became homogeneous in terms of defects distribution, with lower number of micro-interstices. Therefore, the roughness of the surface and the actual surface area of the coatings probably decreased by increasing oxidation time leading to a reduction of the solution resistance.

$CPE_1$ reflects the dielectric behaviour of the interface between electrolyte and coating making it an ideal capacitor C for n = 1. The ideal capacitor is described as $C = C^{\circ}$. A, where $C^{\circ}$ is normalized capacitance and A is the coating exposed area [38,40]. Decreasing the values of $CPE_1$ with the oxidation time showed that A was reduced, which is consistent with the change of the coating morphology observed which will be presented in Section 3. These changes were associated with formation of simonkolleite limiting the supply of oxygen to the zinc substrate,. As the oxidation time was increased, the values of $CPE_1$ increased and n values shifted further from 1, the spreading effect to $CPE_1$ was enhanced, and the capacitive interface was weakened.

The electric charge transfer resistance ($R_2$) relates to the Faraday current to the electrode process. The smaller the value of $R_{ct}$, the better is the interface transfer rates. For the zinc oxalate coating, charges not only transfer between the solution and the coating, but travel throughout the coating layer, so that the $R_{ct}$ value may reflect the ability of transferring the charges of the coating and the compactness of the coating. The $R_{ct}$ value increases as the oxidation time increased, showing that the coating also improves the density with increasing time.

The inner layer of the coating was more compact and less porous, which means that the diffusion resistance of the reagents can be mainly attributed to the inner layer, and thus $CPE_2$ is defined as CPE inner layer, which reflects the variable nature of the inner layer structure. This decrease in $CPE_2$ results from a decrease in local dielectric constant and/or an increase in the thickness of the double layer, suggesting that corrosion products are formed and absorbed at the zinc interface. The reduction in values of $CPE_2$ can be ascribed to an increase in the double electric layer thickness due to the adsorption on the electrode surface.

The increasing of $R_1$ indicates that there is a development of a compact protective film on the electrode surface by the corrosion products formed, thereby enhancing the corrosion resistance of the coating. The increasing of $R_2$ indicates that the charge transfers reactions occurring in the protective film were strongly restricted by the formed corrosion products such as simonkolleite. This reflects that the surface structure is improved and the coating becomes more resistant to the chloride attack, consequently leading to a decrease in corrosion rate. The sum of the resistance values of the coating and the charge transfer resistance of the electric double layer ($R_1 + R_2$) is a way to measure the protective effect as a function of immersion time in chloride solution [40,41], as shown in Fig. 11.

The zinc corrosion resistance increased with the addition of a zinc oxalate coating. The immersion process in oxalic acid solution led to the formation of zinc oxalate conversion coating in conjunction with zinc corrosion products in advanced stage due to acidity of solution. In the initial immersion time (up to 3 days) in sodium chloride solution, the resistance values ($R_1 + R_2$) were quite similar. The low solubility products are anchored at the coating providing a significant increase in corrosion protection.

The electrochemical results obtained after stabilization of the OCP (4 h), with the absence of capacitive loop at high frequencies, show that electrolyte penetration and surface attack occurs relatively quickly (times less than 4 h). To better understand the corrosion mechanism, morphologic and surface characterization analyses (FEG/EDX, XRD,

**Table 4**
EIS fitted parameters of untreated zinc under a NaCl $10^{-1}$ M solution after 4 h, 1 day, 3 days, 5 days and 7 days exposure time.

| Time | Rsol (Ω.cm$^2$) | Error (%) | CPE1 (μF cm$^2$·Hz$^{1-n1}$) | Error (%) | α1 | Error (%) | R1 (Ω cm2) | Error (%) | CPE2 (μF cm$^2$·Hz$^{1-n1}$) | Error (%) | α2 | Error (%) | R2 (Ω cm$^2$) | Error (%) | ZW (μF cm$^2$ Hz0.5) | Error (%) |
|---|---|---|---|---|---|---|---|---|---|---|---|---|---|---|---|---|
| 4 h | 47.35 | 0.12 | 37.0 | 1.78 | 0.96 | 4.63 | 46.41 | 2.98 | 97.5 | 6.78 | 0.82 | 4.31 | 1033 | 6.9 | 610 | 5.1 |
| 1 day | 45.86 | 0.35 | 51.2 | 3.45 | 1 | 4.72 | 34.47 | 1.78 | 708 | 5.99 | 0.58 | 4.02 | 1416 | 8.5 | 910.4 | 7.6 |
| 3 days | 35.7 | 0.67 | 33.7 | 1.65 | 0.72 | 3.99 | 232.3 | 1.61 | 843 | 5.97 | 0.53 | 4.44 | 938.7 | 4.92 | 186.7 | 3.2 |
| 5 days | 32.76 | 0.15 | 131 | 1.20 | 0.82 | 4.00 | 166.4 | 2.13 | 1080 | 6.62 | 0.64 | 4.49 | 685.1 | 1.8 | 669.1 | 2.1 |
| 7 days | 48.34 | 0.38 | 190 | 1.95 | 0.86 | 3.26 | 116 | 2.19 | 1320 | 6.02 | 0.51 | 4.37 | 735.6 | 8.76 | 2030 | 9.4 |

**Table 5**
EIS fitted parameters of zinc oxalate coating (obtained in$10^{-1}$ M oxalic acid solution) under a NaCl $10^{-1}$ M solution after 4 h, 3 days, 5 days and 7 days of exposure time.

| Time | Rs (Ω cm$^2$) | Error (%) | CPE1 (μF cm$^2$ Hz$^{1-n1}$) | Error (%) | α1 | Error (%) | R1 (Ω cm$^2$) | Error (%) | CPE2 (μF cm$^2$ Hz$^{1-n1}$) | Error (%) | α2 | Error (%) | R2 (Ω.cm$^2$) | Error (%) |
|---|---|---|---|---|---|---|---|---|---|---|---|---|---|---|
| 4 h | 59.8 | 0.25 | 214.0 | 1.07 | 0.80 | 0.80 | 33.48 | 3.69 | 2781.5 | 0.96 | 0.51 | 1.01 | 347.5 | 1.02 |
| 1 day | 51.45 | 0.27 | 229.5 | 1.48 | 0.79 | 0.79 | 518.5 | 1.78 | 2135.0 | 2.21 | 0.62 | 1.32 | 169.7 | 1.71 |
| 3 days | 49.5 | 0.33 | 313.3 | 1.2 | 0.77 | 0.31 | 951 | 1.30 | 1156.3 | 2.89 | 0.66 | 0.66 | 264.2 | 1.09 |
| 5 days | 43.99 | 0.28 | 394.6 | 1.08 | 0.75 | 0.32 | 5082 | 0.32 | 439.8 | 3.87 | 0.88 | 0.58 | 6055 | 1.15 |
| 7 days | 43.16 | 0.20 | 493.9 | 1.40 | 0.71 | 0.47 | 6039 | 1.45 | 690 | 4.56 | 0.91 | 3.72 | 6098 | 3.46 |

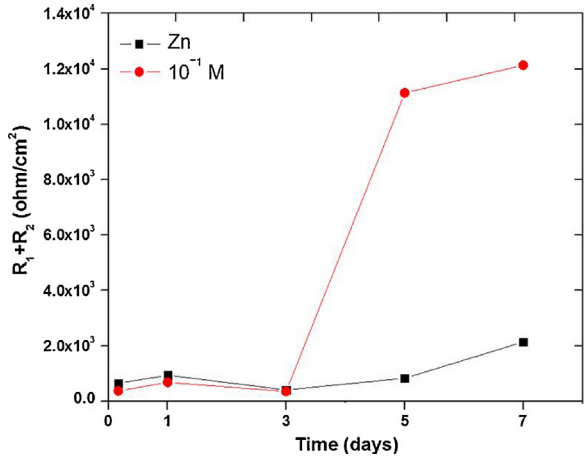


**Fig. 11.** EIS results ($R_1$ + $R_2$) as function of immersion time in corrosive solution for Zinc untreated (Zn) and treated by immersion in oxalic acid solution (Zn + $10^{-1}$ M oxalic acid).

XPS and FIB) were performed after exposure to corrosion medium with lower times (10 min; 30 min and 60 min) and times that show according to the results of EIS be markedly important (3 days, 5 days and 7 days).

### 3.3. After exposure to of $10^{-1}$ M NaCl solution (corrosion test)

#### 3.3.1. Chemical and structural characterization

*3.3.1.1. SEM.* Fig. 12 shows SEM images of zinc oxalate for (a) uncorroded and after various periods of exposure to $10^{-1}$ M NaCl solution, specifically (b) 10 min; (c) 30 min and (d) 60 min.

From the first moments of contact with the corrosive solution, the porosity of the oxalate layer allows the infiltration of sodium chloride solution and formation of the first zinc corrosion products, which apparently grow from the substrate towards the surface through the oxalate coating. Sequentially, the first hour of immersion in corrosive solution exposure to long periods of time allows the observation of significant changes in surface morphology. These changes are shown in Fig. 13, with SEM images of zinc surface treated in $10^{-1}$ M oxalic acid after various periods of exposure to $10^{-1}$ M NaCl solution, specifically (a) 4 h; (b) 3 days (c) 5 days and (d) 7 days.

SEM images for treated samples reveal significant changes in the surface morphology with time of immersion, suggesting an increase of dissolution of the deposited oxalate coating on the corrosive medium ($10^{-1}$ M NaCl) and resulting in a smoother and more regular surface (Fig. 13a–d). It is proposed that intense attack at the metallic zinc substrate underneath the porosities of the coating results in increasing removal of the coating and the local pH increase leads to zinc hydroxide dissolution and consequently zincate ions formation. Exposure of the treated samples to the corrosive solution resulted in uniform attack of the surface. On the other hand, zinc untreated samples exposed to the same corrosive solution showed intense localized attack after few days of immersion. Therefore, it can be concluded that the oxalate coating prevented localized corrosion by distributing the corrosion currents throughout the surface but the local conditions underneath the coating resulted in its increasing attack. Results of EDX analysis obtained at the surface of zinc treated in $10^{-1}$ M of oxalic acid solution after exposure for 3, 5 and 7 days in $10^{-1}$ M NaCl solution are summarized in Table 6.

It was also possible to observe that electrolytic solution components, sodium and chloride ions promote surface attack and form detectable compounds only after 5 days of exposure.

*3.3.1.2. XRD.* Fig. 14 shows XRD diffractograms for (a) zinc untreated surface after 7 days exposure to chloride solution, (b) zinc surface treated in $10^{-1}$ M oxalic acid solution after 5 days and (c) after 7 days

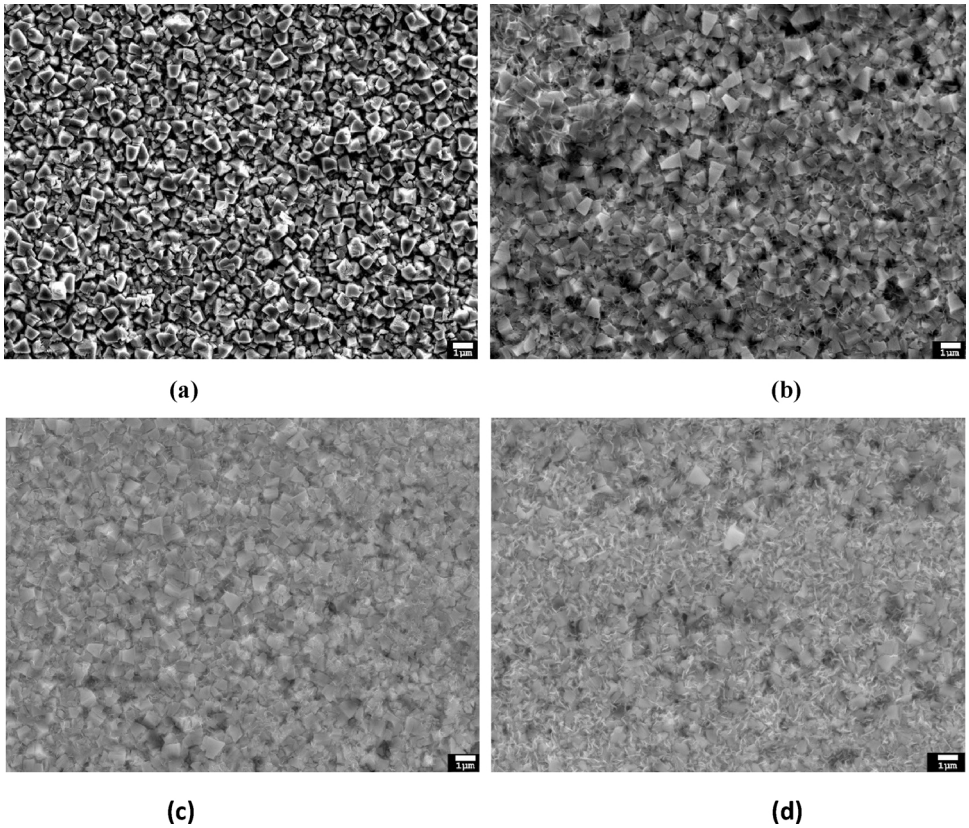


**Fig. 12.** Zinc oxalate coating micrographs for (a) uncorroded sample, and after exposure to corrosive solution (NaCl $10^{-1}$ M) for (b) 10 min; (c) 30 min and (d) 60 min.

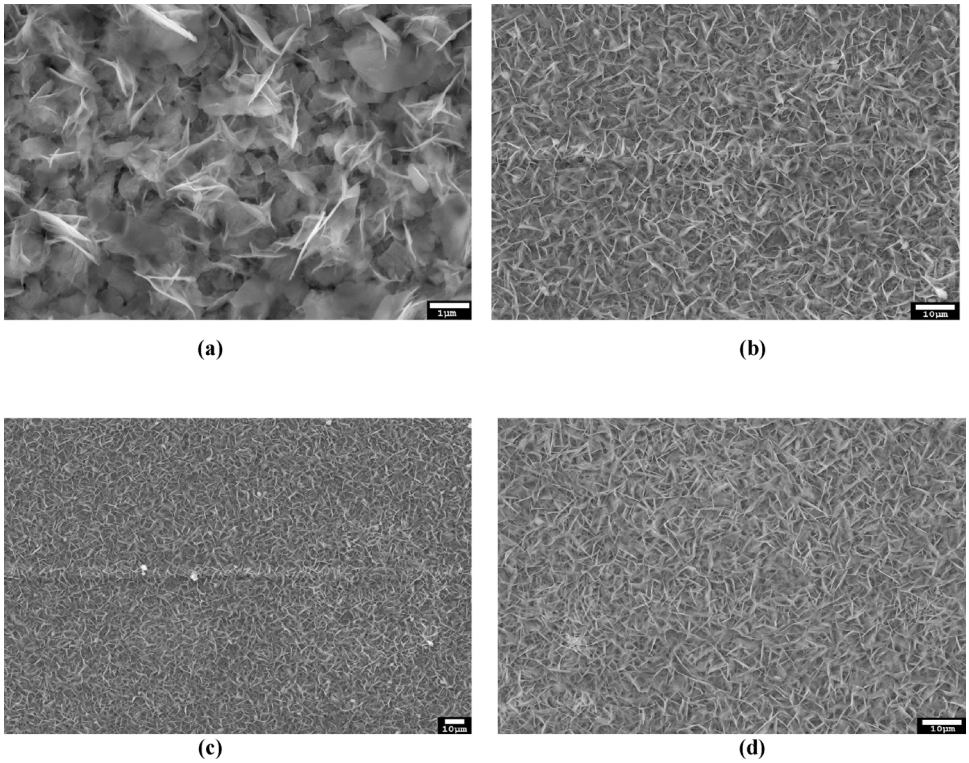


**Fig. 13.** SEM images of zinc surface treated in $10^{-1}$ M oxalic acid exposed to $10^{-1}$ M NaCl solution for (a) 4 hours (b) 3 days, (c) 5 days and (d) 7 days.

**Table 6**
EDX results showing the atomic concentrations at the surface zinc coupons treated by immersion in $10^{-1}$ M of oxalic acid after exposure to chloride solutions for 3 days, 5 days and 7 days.

| Time (days) | C K | O K | Zn L | Na K | Cl K |
|---|---|---|---|---|---|
| **3** | 38.25 | 46.53 | 15.22 | – | – |
| **5** | 30.78 | 27.64 | 32.59 | 5.81 | 3.18 |
| **7** | 23.12 | 30.13 | 28.14 | 12.16 | 6.45 |

of exposure to chloride solution.

XRD results show that, in all samples, Zn° phase (I) is present, related to the metallic zinc substrate. Zinc oxide (II) was also observed in samples untreated and oxalate coating after 7 days of corrosion, related to the attack of the corrosive solution for long periods of time. Zinc hydroxide (III) was found on oxalate coating after 7 days of corrosion. Zinc hydroxide chloride hydrated or simonkolleite ($Zn_5(OH)_8Cl_2{\cdot}H_2O$) (IV) is a zinc corrosion product responsible for reducing the rate of corrosion, which is considered an anticorrosive layer. As observed in the initial times of immersion in corrosive medium, the penetration of the electrolyte is fast and promotes at equivalent times, formation of ($Zn_5(OH)_8Cl_2{\cdot}H_2O$) in samples treated after 5 and 7 days. These results corroborate with the electrochemical results where the highest impedance values are associated with corrosion product known to cause zinc protection. The difference in impedance values of the treated sample with oxalate coating after 3, 5 and 7 days may be associated with the amount of product ($Zn_5(OH)_8Cl_2{\cdot}H_2O$) formed and in this case the treatment with oxalic acid at specific concentration is pointed as an agent accelerator to ($Zn_5(OH)_8Cl_2{\cdot}H_2O$) not formed in an equivalent corrosion time to zinc untreated.

*3.3.1.3. XPS.* XPS high resolution scans for C 1s, O 1s, Zn 2p, Zn LMM and Na 1s peaks for the zinc oxalate samples $10^{-1}$ M after immersion in NaCl solution $10^{-1}$ M are presented in Fig. 15. The peaks were quantified and the results are shown in Table 7.

The results for the C 1 s peak prior to and after corrosion are qualitatively similar. XPS results show two main components, 285.0 eV and 289.4 eV, associated respectively with aliphatic carbon (C—C/C—H), and carbon of carboxyl group (—COOH) and/or carbonate ($-CO_3^{2-}$). Due to the absence of aliphatic carbon in the oxalate structure, the peak observed at 285.0 eV is considered contamination and its intensity decreases with exposure time to chloride solution.

The XPS analyses probe only a few nanometers in depth and the presence of chlorine observed by XRD and not observed in the results of XPS is an argument for simonkolleite formation exclusively at the interface zinc/zinc oxalate.

Prior to exposure to corrosive solution, the samples presented small amounts of aliphatic carbon (see Fig. 5a). After the first few days of exposure, there is an increase of the peak at 285.0 eV, showing that the surface is not stable, and corrosion products have been formed. After 5 days of exposure to NaCl solution, the peak at 285.0 eV decreases due to the formation of more stable corrosion products. Such increase in stability is due to high levels of oxidation, observed in the O 1s peak, which evolves from oxide through hydroxide to carbonate over days of exposure.

The XPS spectra of the Zn $2p_{3/2}$ peaks of the zinc oxalate $10^{-1}$ M samples after 4 h and 1 day exposure time to corrosive solution are shown in Fig. 15c, which contain a single peak located at 1021.3 eV. This single peak was symmetric, ruling out the existence of Zn in multiple chemical states. The Zn $2p_{3/2}$ peak positions closely matched the standard value of ZnO, indicating that the Zn atoms were in the $2^+$ oxidation state [27,34].

The same behaviour is observed for the Zn 2p peaks, which starts as metallic zinc (1021.2 eV) and evolves to $ZnCO_3/Zn(OH)_2$ (1023.9 eV). The peaks between 1018 eV to 1020 eV are reported as impurities and can be linked to sodium compounds formed by corrosion.

The reactions leading to the corrosion products identified on the surface are indicated in Eqs. (4)– (6). Local pH increase at the cathodic sites reacts with the corrosion products and forms zincate ions (Eq. (7)) solubilizing the corrosion product. In chloride medium, eventually chloride ions migrate to anodic sites and simonkolleite is formed (Eq. 8)

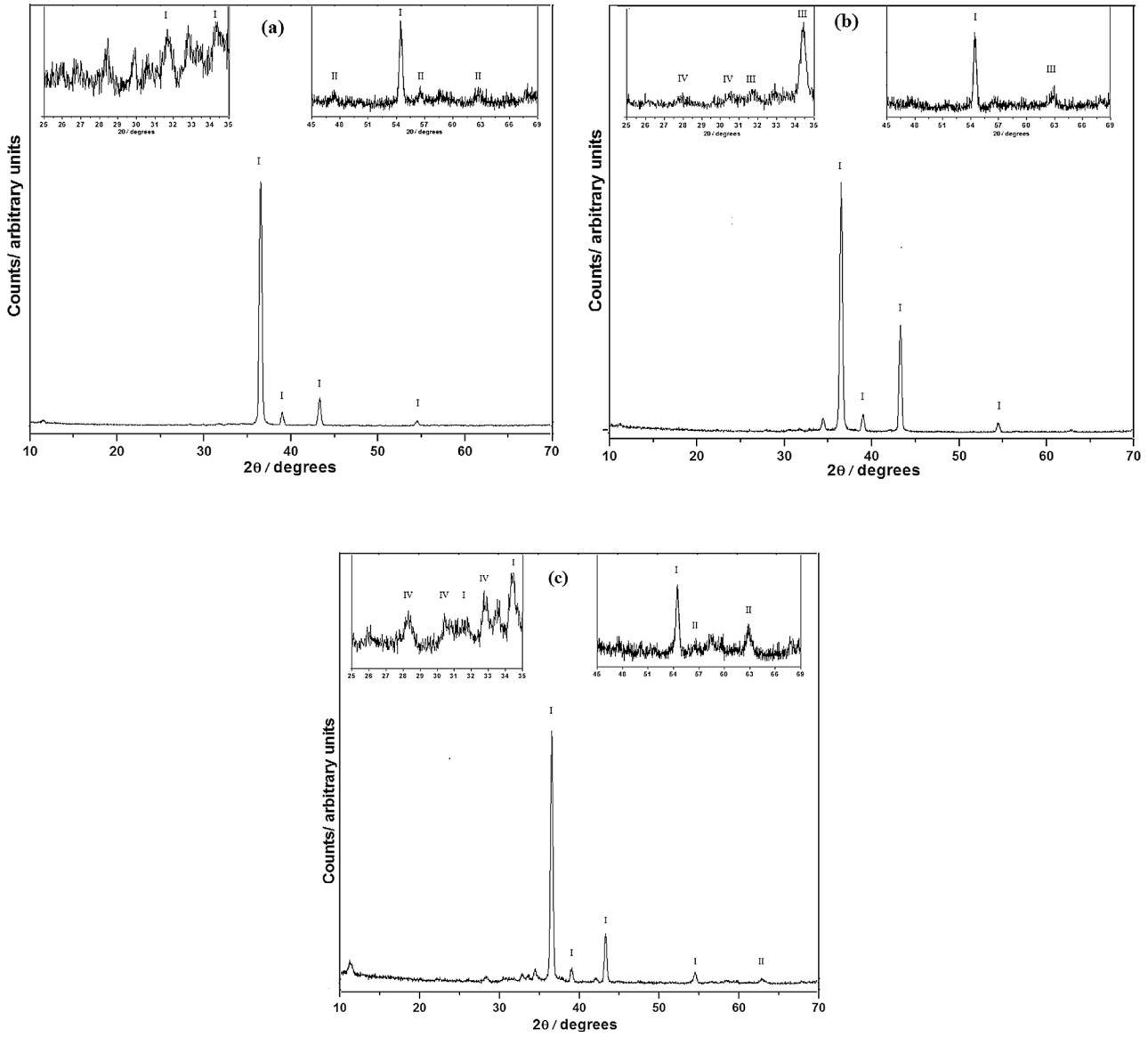


**Fig. 14.** XRD diffractograms of zinc surface (a) without surface treatment and exposed for 7 days to $10^{-1}$ M NaCl solution; (b) treated in $10^{-1}$ M oxalic acid and exposed for 5 days and (c) 7 days to chloride solution.

[41–44]. This occurred for the untreated sample exposed to the corrosive solution but was not evident for the treated ones after 7 days of exposure, with only slight indication seen in the XPS spectra.

$$O_2 + 2H_2O + 4e^- \rightarrow 4OH^-_{(aq)} \quad (4)$$

$$Zn^0 \rightarrow Zn^{2+} + 2e^- \quad (5)$$

$$Zn^{2+} + 2OH^- \rightarrow Zn(OH)_2 \quad (6)$$

$$Zn(OH)_2 + 2OH^- \rightarrow Zn(OH)_4{}^{2-} \quad (7)$$

$$5Zn(OH)_2 + 2Cl^- + H_2O \rightarrow 5Zn_5(OH)_8Cl_2 + 2OH^- \quad (8)$$

The presence of zinc carbonate was also detected by XPS after 5 days and 7 days of exposure to NaCl solution. The formation of these products depends on the dissolution of atmospheric carbon dioxide into the corrosion solution electrolyte, as shown in Eqs. (9) and (10) [41,42,44].

$$CO_2\ (aq) + 2OH^-\ (aq) \rightarrow CO_3{}^{2-}\ (aq) + H_2O \quad (9)$$

$$CO_2\ (aq) + CO_3{}^{2-} + H_2O \rightarrow 2HCO_3\text{-}(aq) \quad (10)$$

The Na 1 s peak was fitted in three components at ~1071.0 eV, ~1071.2 eV and 1072.2 eV corresponding respectively to sodium oxalate ($Na_2C_2O_4$), sodium bicarbonate ($NaHCO_3$) and sodium carbonate ($Na_2CO_3$). The reaction at cathodic areas between sodium ions ($Na^+$) and carbonate ions forms hydroxide carbonate and sodium carbonate (Eqs. (11) and (12)) [45,46].

$$Na^+ + HCO_3{}^- \rightarrow NaHCO_3 \quad (11)$$

$$Na^+ + NaHCO_3 \rightarrow Na_2CO_3 + H^+ \quad (12)$$

According to the XPS results, a layer containing sodium carbonate/bicarbonate and sodium oxalate is formed after 5 days and 7 days of exposure to sodium chloride solution. The zinc and oxygen ratio show that the surfaces of zinc oxalate were enriched with oxygen when exposed to air and humidity. Once the oxalate layer was exposed to corrosive solution, sodium chloride is the activation of the surface and the values of the ratio zinc and oxygen (Zn/O) on the surface are increased. The longer period of exposure allowed the formation of zinc hydroxide and simonkolleite. Excess oxygen can be explained by the presence of other carbonates, such as sodium carbonate on the surface of the sample.

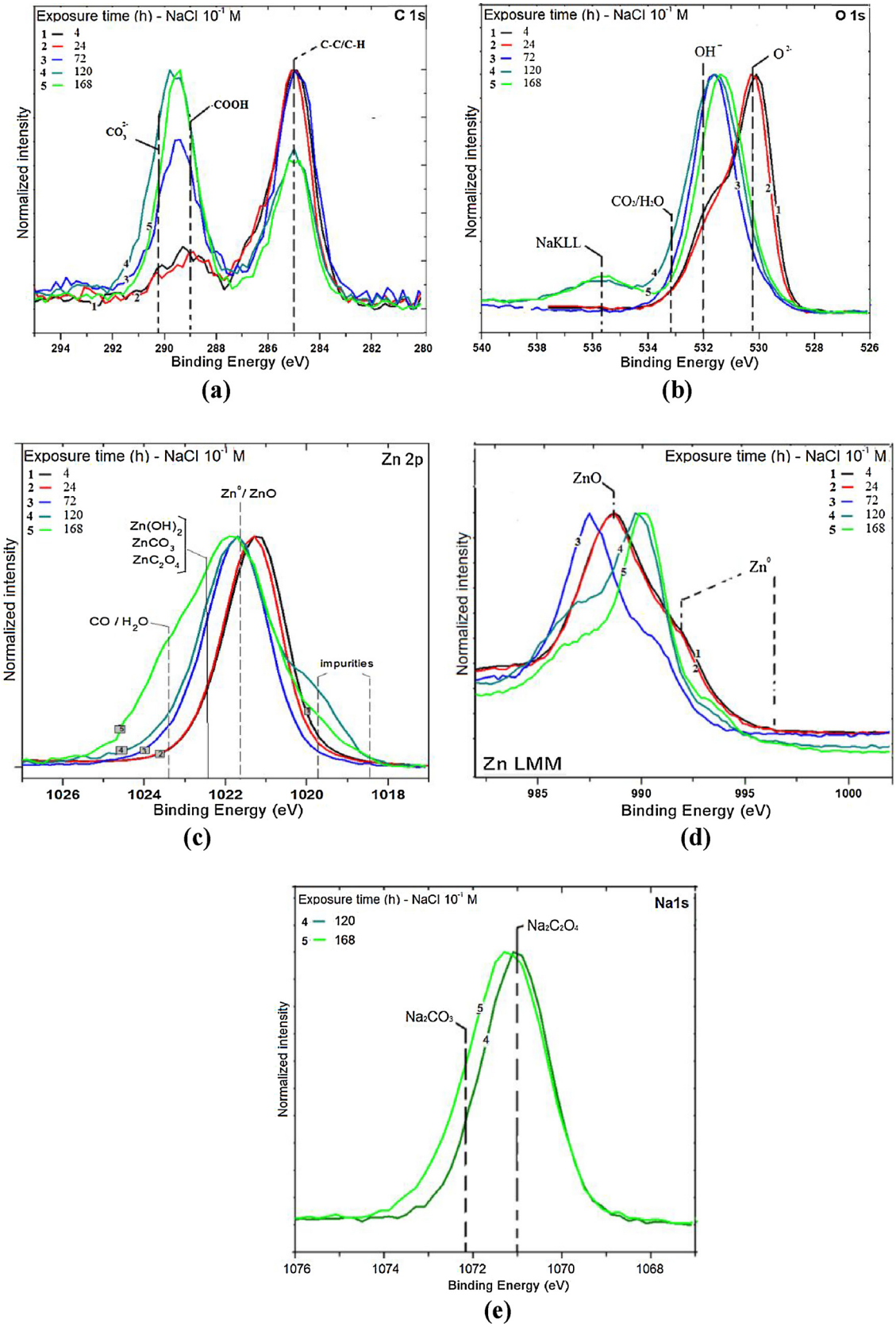


**Fig. 15.** Overlay of XPS high-resolution spectra for the zinc oxalate sample $10^{-1}$ M to various times of exposure to $10^{-1}$ M chloride solution: (a) carbon (C 1 s); (b) oxygen (O 1 s); (c) zinc (Zn 2p3/2), (d) zinc Auger (Zn L3M45N45) and (e) sodium (Na 1s).

**Table 7**
XPS peak binding energies and elemental concentrations observed for the zinc oxalate sample after immersion in NaCl solution $10^{-1}$ M.

| TIME (h) | XPS peak | BE(eV) | Elemental concentration (at.%) |
|---|---|---|---|
| **4** | **C 1 s** | 285.0 | 12.91 |
| | **O1 s** | 530.2 | 45.35 |
| | **Zn $2p_{3/2}$** | 1021.2 | 41.73 |
| **24** | **C 1 s** | 285.0 | 13.77 |
| | **O1 s** | 530.28 | 44.46 |
| | **Zn $2p_{3/2}$** | 1021.3 | 41.47 |
| **72** | **C 1 s** | 285.0 | 19.09 |
| | **O1 s** | 531.6 | 50.18 |
| | **Zn $2p_{3/2}$** | 1021.7 | 30.73 |
| **120** | **C 1 s** | 289.4 | 19.68 |
| | **O1 s** | 531.0 | 44.16 |
| | **Zn $2p_{3/2}$** | 1022.8 | 12.52 |
| | **Na 1 s** | 1071.0 | 23.63 |
| **168** | **C 1 s** | 289.5 | 18.3 |
| | **O1 s** | 531.6 | 44.71 |
| | **Zn $2p_{3/2}$** | 1021.9 | 9.23 |
| | **Na 1 s** | 1071.2 | 27.76 |

The nature of the inhibitive effect of a zinc oxalate coating containing carbonate and/or zinc oxide is not completely clear. The passivity of the zinc oxalate coating is mainly due to the presence of corrosion products that limit the transport of chloride ions. This may occur due to larger charge density that improves the retention of the carbonate or by the repulsion of chloride ions by the negatively charged surface film. The different behaviour of zinc under zinc oxalate coating in NaCl electrolyte seems to be related to differences in the ion-exchange properties of the outer layer. In this case, small amounts of defect size resulted in a slower drying rate and a more restricted diffusion of oxygen into the pores as observed in SEM images (Fig. 13). Consequently, the oxygen reduction was slower, which favoured the formation of simonkolleite in function of immersion time in sodium chloride solution. At this point in the work it was possible to verify that some questions should be answered, such as: Does the formation of corrosion products occur along the oxalate layer? In this process, is the oxalate layer consumed? How is the distribution of the elements of the electrolytic solution in the oxalate layer? These questions were answered by the acquisition of XPS depth profiles for oxalate samples prior to exposure to corrosive sodium chloride solution and after exposure for different times from 10 min to 7 days, as shown in Fig. 16 and also by the acquisition of FIB/SEM images, present in Fig. 17.

The organic coating is represented by the carbon profile (carboxyl peak at 289 eV). It can be observed that the coating is thicker for the less corroded samples and becomes much thinner for the most corroded sample (7 days). This shows that the oxalate coating is consumed throughout the corrosion process. The presence of oxygen after the disappearance of carbon for all samples, confirms that the organic coating is in fact adsorbed onto an oxide layer.

Regarding the signals for the ions present in the electrolyte ($Na^+$ and $Cl^-$), sodium is observed for all samples and at all sputter levels, including the oxide-metal interface. Chlorine, on the other hand, is only observed after 60 min corrosion time and much more intense for the sample corroded for 7 days, which agrees to the XRD results that showed the pattern for simonkolleite ($5Zn_5(OH)_8Cl_2$). At the last profiles sputter levels (250), the higher O/Zn ratio for the sample corroded for 7 days shows that the corrosion products layer formed is thicker than in the samples with less corrosion time.

The XPS depth profiling results show that, prior to corrosion (Fig. 16a), oxalate layer is bonded to the zinc oxide due to the disappearance of the carbon signal at the 150 sputter levels where the O/Zn ratio is 1:1. The increase of the exposure time to sodium chloride solution promotes the gradual consumption of the oxalate layer, however, even after seven days of corrosion, there is still an oxalate layer. It is important to note that the carbon peaks observed along the sputter levels in all depth profiles are related to the carboxylic group (289 eV), with the peak referring to contaminant and aliphatic carbon (285 eV) removed after the first sputter levels.

Sodium has easy penetration through the oxalate layer and reaches the interface Zinc/oxalate coating after 10 min of immersion and remains throughout the immersion time in a corrosive solution of sodium chloride. As can be observed after 7 days of corrosion where the amount of this element is higher than the amount of chloride. shows a slower penetration, compared to sodium, after one hour (Fig. 16d) it is possible to observe the first signs of chloride. In the following times of corrosion, the chloride signal is followed by noise and should be better understood in the future. However, it is possible to observe that after seven days of corrosion the chlorine signal is more intense in the final etch sputter levels, an argument for the presence chloride in the form of simonkolleite as described in the results of XRD (Fig. 14c).

The use of the same etch parameters allowed a comparison between the different XPS depth profiles as a function of the corrosion time. From the profile for the zinc signal, which reaches high concentrations and represents metallic zinc for the substrate, it can be stated that, after seven days of corrosion, the layer is practically homogeneous with respect to its constituents and that these products are more stable and difficult to be removed by the argon ions.

*3.3.1.4. Focused ion beam.* Fig. 17 shows FIB images obtained for oxalate zinc layers before and after different corrosion and zinc times after 7 days of corrosion. It is possible to observe that the zinc oxalate layer ($10^{-1}$ M), prior to corrosion, is porous and has uniform thickness (Fig. 17a).

The attack of the oxalate layer by sodium chloride makes the coating more porous and thicker by the third day. However, after the third day the coating becomes thinner, more compact and the porosity decreases from the fifth to the seventh day of corrosion. These results are in agreement with the XPS depth profiles (Fig. 16) where it was observed a layer more stable and difficult to be removed by the argon ions.

After 30 min of exposure, the corrosive attack of the zinc oxalate layer that led to the formation of pores in the crystallites can be seen in Fig. 17b. The first layer in which the zinc surface was attacked, contains both zinc and zinc oxide. Although not particularly apparent from this image, there is a second crystalline layer that shows a significant fraction of pores and voids. Thus, FIB results indicate a double layer of oxides. Neufeld et al. [43] observed that the level of porosity in zinc oxide decreases with time and, because of the accumulation of thicker and more compact oxide areas, it can change from anode to cathode. Thus, a detailed knowledge of the thickness, porosity and oxide composition is essential for understanding the corrosion process and then for designing possible interventions to limit this process.

### *3.4. Corrosion mechanism*

The morphological and chemical results before and after the corrosion enabled better understanding of the mechanism of zinc oxalate coating formation, which can be described by a mechanism of corrosion that suggests the formation of. simonkolleite during the corrosion of the $10^{-1}$ M oxalate coating after 5 days of immersion on corrosive mediumSuch proposed corrosion mechanism is shown in the schematics of Fig. 18.

The coating model proposed is a porous layer where the attack occurs in pores and drives the hydroxyl ions to neighbour regions to anodic sites, causing break-up of the oxalate coating and forming carbonate ions plus hydroxyl ions. Those ions react with zinc oxalate, forming zinc ions complexes such as simonkolleite.

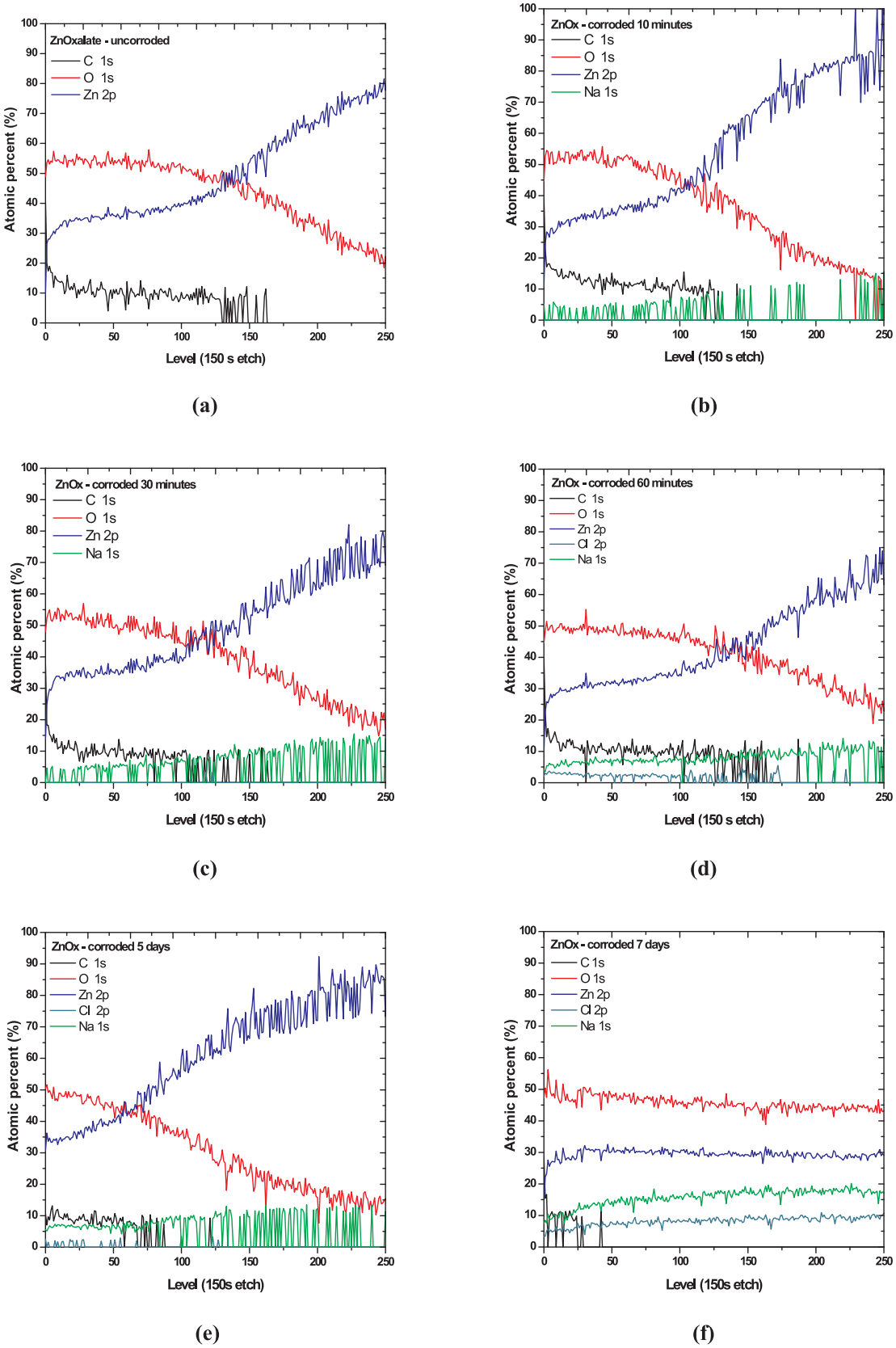


**Fig. 16.** XPS depth profile of zinc oxalate coating (a) uncorroded and corroded with different times (b) 10 min; (c) 30 min; (d) 60 min; (e) 5 days and (f) 7 days.

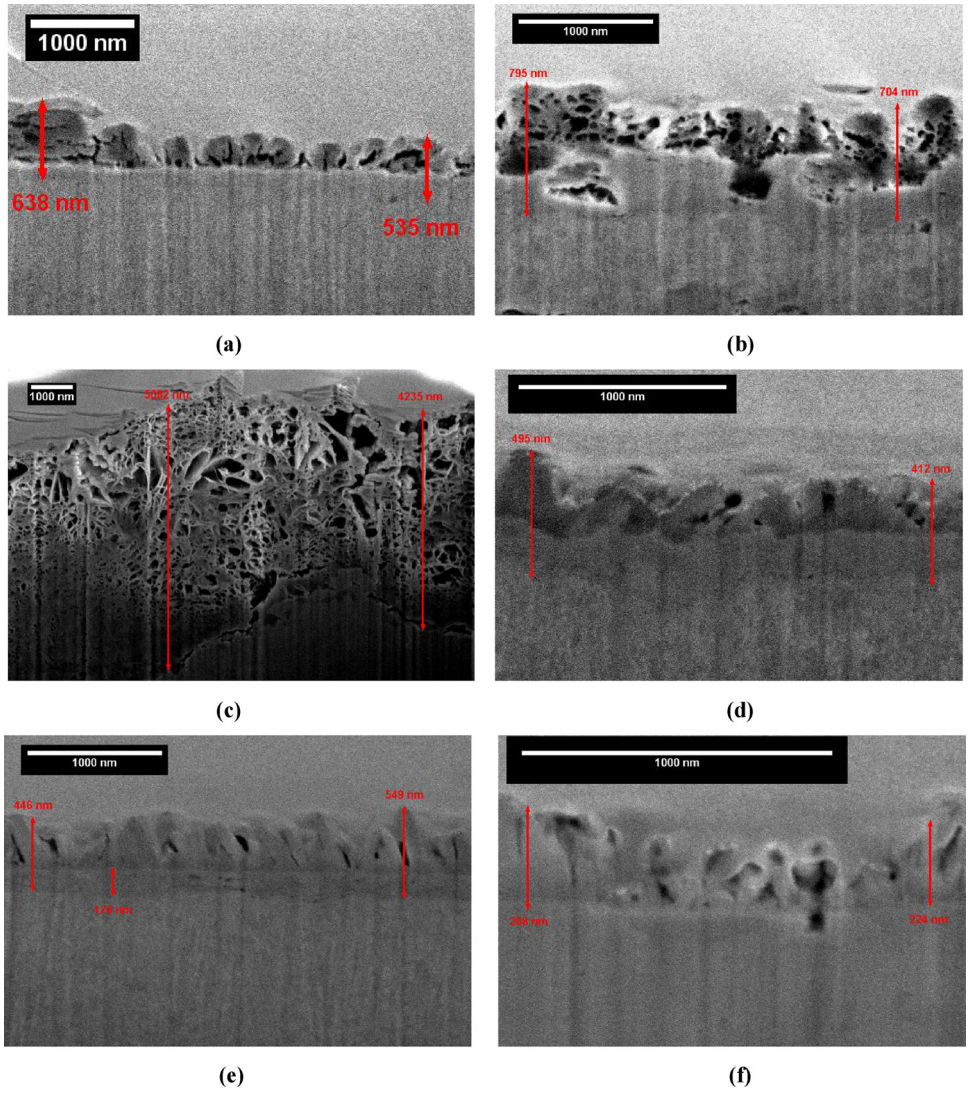


**Fig. 17.** FIB images of oxalate coating $10^{-1}$ M (a) uncorroded and corroded with different times (b) 30 min; (c) 3 days; (d) 5 days and (e) 7 days and (f) untreated zinc corroded for 7 days.

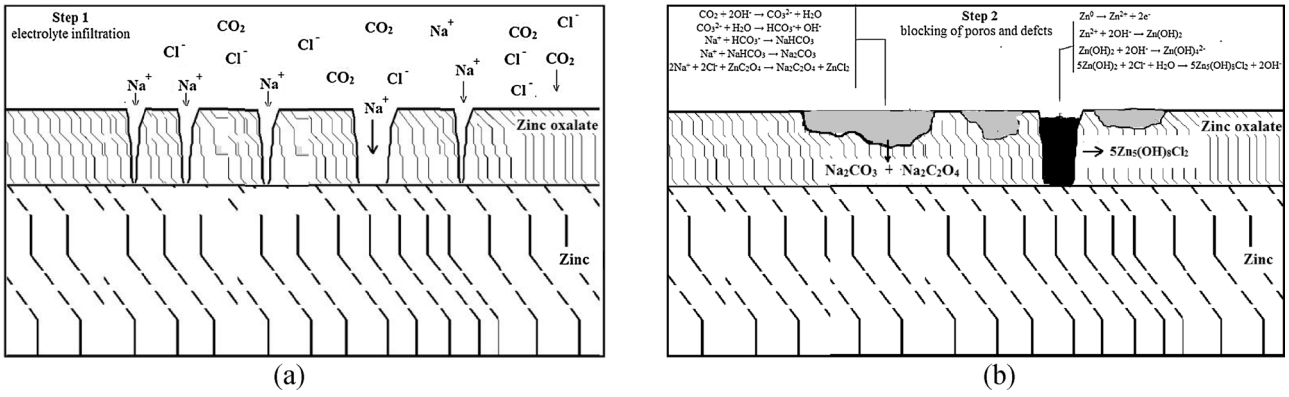


**Fig. 18.** Schematic of the corrosion process of a zinc oxalate layer exposed to sodium chloride.

## 4. Conclusions

This work described the formation of a passive zinc oxalate coating containing a mix of zinc corrosion products formed in oxalate media. The optimum ratio between pH to dissolution of zinc and concentration of oxalate ion to deposition of zinc oxalate were found for the solution concentration $10^{-1}$ M and consequently pH 1.75.

For samples observed as more protective, the composition is predominantly zinc oxalate. The interaction of the carboxylate groups in this case was predominantly of the monodentate type and, although these samples were more protective, this effect was not associated with corrosion protection due to the presence of other modes such as bridge

bidentate, carbonates and oxalic acid fragments.

The zinc oxalate coatings showed effective protection against corrosion and this is mainly due to the formation of simonkolleite from the base of the pores until their completion. It was proposed that zinc corrosion products block pores and forming a barrier protection for the higher exposure times to chloride solution.

Consumption of zinc oxalate layer occurs and the products formed also represent a form of corrosion protection. The consumption of the oxalate layer in the electrolytic solution and the enrichment of the corrosion product by Na with corrosion time were observed and an experiment to investigate such effect is aimed as future work. The effect of zinc corrosion products by consumption of the conversion coating justifies the treatment of immersion of zinc in oxalic acid solution under the ideal conditions identified in this study.

## Acknowledgements

The authors wish to thank CNPq (process 200490/2014-1), CAPES (project: 11995-13-0) and FAPESP (Process 15/09952-0 and 16/504554-6) for financial support of this research. Special thanks to Steven Hinder, David Cox, Dan Driscol David Jones and John F. Watts.

## References

[1] J. Peultier, E. Rocca, J. Steinmetz, Zinc carboxylating: a new conversion treatment of zinc, Corros. Sci. 45 (8) (2003) pp1703–1716.
[2] E. Rocca, J. Steinmetz, Inhibition of lead corrosion with saturated linear aliphatic chain monocarboxylates of sodium, Corros. Sci. 43 (5) (2001) 891–902.
[3] E. Constantinescu, E. Heitz, On the influence of the water content on corrosion of metals in mono-carboxylic acids, Corros. Sci. 16 (11) (1976) 857–867.
[4] U. Rammelt, S. Koehler, G. Reinhard, Electrochemical characterisation of the ability of dicarboxylic acid salts to the corrosion inhibition of mild steel in aqueous solutions, Corros. Sci. 53 (11) (2011) 3515–3520.
[5] E. Constantinescu, E. Heitz, On the influence of the water content on corrosion of metals in mono-carboxylic acids, Corros. Sci. 16 (11) (1976) 857–867.
[6] Y. Li, C. Tan, G. Qi, J. Guo, X. Wang, S. Zhang, Decanoate conversion layer with improved corrosion protection for magnesium alloy, Corros. Sci. 70 (2013) 229–234.
[7] M. Itagaki, A. Ono, K. Watanabe, H. Katayama, K. Noda, Analysis on organic film degradation by dynamic impedance measurements, Corros. Sci. 48 (11) (2006) 3802–3811.
[8] K. Aramaki, T. Shimura, Self-assembled monolayers of carboxylate ions on passivated iron for preventing passive film breakdown, Corros. Sci. 46 (2) (2004) 313–328.
[9] C. Corfias, N. Pebere, C. Lacabanne, Characterization of protective coatings by electrochemical impedance spectroscopy and a thermostimulated current method: influence of the polymer binder, Corros. Sci. 42 (8) (2000) 1337–1350.
[10] S. Yuan, S.O. Pehkonen, B. Liang, Y.P. Ting, K.G. Neoh, E.T. Kang, Superhydrophobic fluoropolymer-modified copper surface via surface graft polymerisation for corrosion protection, Corros. Sci. 53 (9) (2011) 2738–2747.
[11] V.K. Gouda, E.N. Rizkalla, S. Abd-El-Wahab, E.M. Ibrahim, Corrosion behaviour in organic acid solutions—I. Tin electrode, Corros. Sci. 21 (1) (1981) 1–15.
[12] M.C. D'Antonio, A. Wladimirsky, D. Palacios, L. Coggiolaa, A.C. González-Baró, E.J. Baran, R.C. Mercader, Spectroscopic investigations of iron (II) and iron (III) oxalates, J. Braz. Chem. Soc. 20 (3) (2009) 445–450.
[13] M.S. Shoichet, T.J. McCarthy, Convenient syntheses of carboxylic acid functionalized fluoropolymer surfaces, Macromolecules 24 (5) (1991) 982–986.
[14] B. Zhang, T. Kong, W. Xu, R. Su, Y. Gao, G. Cheng, Surface functionalization of zinc oxide by carboxyalkylphosphonic acid self-assembled monolayers, Langmuir 26 (6) (2010) 4514–4522.
[15] G. Reinhard, M. Radtke, U. Rammelt, On the role of the salts of weak acids in the chemical passivation of iron and steel in aqueous solutions, Corros. Sci. 33 (2) (1992) 307–313.
[16] M.M. Hefny, A.G. Gad-Allah, S.A. Salih, M.S. El-Basiouny, Zinc Passivation in oxalate solution, Corrosion 44 (1988) 691–695.
[17] Oxalic acid treatment of carbon steel, galvanized steel and aluminum surfaces, US patent US 4316752 A claimed in 1980 and pubished in 1982 (https://www.google.com/patents/US4316752).
[18] Oxalate as a pretreatment for phosphating, US patent US2164042 A deposited in 1938 and published in 1939 (https://www.google.com/patents/US2164042).
[19] B. Díaz, E. Härkönen, J. Światowska, V. Maurice, A. Seyeux, P. Marcus, M. Ritala, Low-temperature atomic layer deposition of Al2O3 thin coatings for corrosion protection of steel: surface and electrochemical analysis, Corros. Sci. 53 (6) (2011) 2168–2175.
[20] A. Benninghoven, Chemical analysis of inorganic and organic surfaces and thin films by static time-of-flight secondary ion mass spectrometry (TOF-SIMS), Angew. Chem. Int. Ed. 33 (10) (1994) 1023–1043.
[21] A.V. Ghule, K. Ghule, C.Y. Chen, W.Y. Chen, S.H. Tzing, H. Chang, Y.C. Ling, In situ thermo-TOF-SIMS study of thermal decomposition of zinc acetate dihydrate, J. Mass Spectrom. 39 (10) (2004) 1202–1208.
[22] G.F. Trindade, Master Thesis, Surface Modifications in Polymers by Ion Beams for the Study of Biocompatibility, University of Sao Paulo, 2013.
[23] J.M. Ferreira, K.P. Souza, F.M. Queiroz, I. Costa, C.R. Tomachuk, Electrochemical and chemical characterization of electrodeposited zinc surface exposed to new surface treatments, Surf. Coat. Tech 294 (2016) 36–46.
[24] M.M. Chehimi, J.F. Watts, XPS investigations of acid-base interactions in adhesion. Part 3. Evidence for orientation of carbonyl groups from poly(methylmethacrylate) (PMMA) at the PMMA-glass and PMMA-SiO2 interfaces, J. Electron. Spectrosc. 63 (4) (1993) 393–407.
[25] J.M. Ferreira Jr, K.P. Souza, J.L. Rossi, I. Costa, G.F. Trindade, C.R. Tomachuk, Corrosion protection of electrogalvanized steel by surface treatments containing cerium and Niobium compounds, Int. J. Electrochem. Sci. 11 (2016) 6655.
[26] L.S. Dake, D.R. Baer, J.M. Zachara, Auger parameter measurements of zinc compounds relevant to zinc transport in the environment, Surf. Interface. Anal. 14 (1–2) (1989) 71–75.
[27] S. Aksela, J. Väyrynen, H. Aksela, High-Resolution Auger spectrum of free zinc atoms, Phys. Rev. Lett. 33 (17) (1974) 999.
[28] R.G. Buchheit, M. Cunningham, H. Jensen, M.W. Kendig, M.A. Martinez, A correlation between salt spray and electrochemical impedance spectroscopy test results for conversion-coated aluminum alloys, Corrosion 54 (1) (1998) 61–72.
[29] M.K. Sinha, S. Pramanik, S.K. Sahu, L.B. Prasad, M.K. Jha, B.D. Pandey, Development of an efficient process for the recovery of zinc and iron as value added products from the waste chloride solution, Sep. Purif. Technol. 167 (2016) 37–44.
[30] K. Aramaki, T. Shimura, Self-assembled monolayers of carboxylate ions on passivated iron for preventing passive film breakdown, Corros. Sci. 46 (2) (2004) 313–328.
[31] X. Bai, T.H. Tran, D. Yu, A. Vimalanandan, X. Hu, M. Rohwerder, Novel conducting polymer based composite coatings for corrosion protection of zinc, Corros. Sci. 95 (2015) 110–116.
[32] K. Aramaki, Effects of organic inhibitors on corrosion of zinc in an aerated 0.5 M NaCl solution, Corros. Sci. 43 (10) (2001) 1985–2000.
[33] E. Rocca, C. Caillet, A. Mesbah, M. Francois, J. Steinmetz, Intercalation in zinc-layered hydroxide: zinc hydroxyheptanoate used as protective material on zinc, Chem. Mater. 18 (26) (2006) 6186–6193.
[34] M. Lebrini, G. Fontaine, L. Gengembre, M. Traisnel, O. Lerasle, N. Genet, Corrosion protection of galvanized steel and electroplating steel by decanoïc acid in aqueous solution: Electrochemical impedance spectroscopy, XPS and ATR-FTIR, Corros. Sci. 51 (6) (2009) 1201–1206.
[35] J.R. Macdonald, Impedance Spectroscopy V 11 Wiley, New York, 1987.
[36] E. Barsoukov, J.R. Macdonald (Eds.), Impedance Spectroscopy: Theory, Experiment, and Applications, John Wiley & Sons, 2005.
[37] C. Compere, E. Fréchette, E. Ghali, The corrosion evaluation of painted and artificially damaged painted steel panels by AC impedance measurements, Corros. Sci. 34 (8) (1993) 1259–1274.
[38] X.G. Zhang, Corrosion and Electrochemistry of Zinc, Springer Science & Business Media, 2013.
[39] G. Quartarone, M. Battilana, L. Bonaldo, T. Tortato, Investigation of the inhibition effect of indole-3-carboxylic acid on the copper corrosion in 0.5 M H2SO4, Corros. Sci. 50 (12) (2008) 3467–3474.
[40] F.C. Porter, Corrosion Resistance of Zinc and Zinc Alloys, CRC Press, 1994.
[41] Y. Chen, S.C. Chung, H. Shih, Studies on the initial stages of zinc atmospheric corrosion in the presence of chloride, Corros. Sci. 48 (11) (2006) 3547–3564.
[42] Z.Y. Chen, D. Persson, C. Leygraf, Initial NaCl-particle induced atmospheric corrosion of zinc—Effect of CO2 and SO2, Corros. Sci. 50 (1) (2008) 111–123.
[43] A.K. Neufeld, I.S. Cole, A.M. Bond, S.A. Furman, The initiation mechanism of corrosion of zinc by sodium chloride particle deposition, Corros. Sci. 44 (3) (2002) 555–572.
[44] M. Mouanga, P. Berçot, J.Y. Rauch, Comparison of corrosion behaviour of zinc in NaCl and in NaOH solutions. Part I: corrosion layer characterization, Corros. Sci. 52 (12) (2010) 3984–3992.
[45] A. Shchukarev, D. Korolkov, XPS study of group IA carbonates, Open. Chem. 2 (2) (2004) 347–362.
[46] J.S. Hammond, J.W. Holubka, R.A. Dickie, The application of x-ray photo-electron spectroscopy to a study of interfacial composition in corrosion-induced paint de-adhesion, Corros. Sci. 21 (3) (1981) 239–253.